Bachelor Mathematics

Track: Biomedical Mathematics

*Bachelor thesis*

# Mathematical modeling of ventricular fibrillation via calcium overload

by

Erik Bosch

July 1, 2017

Supervisor: dr. Bob Planqué

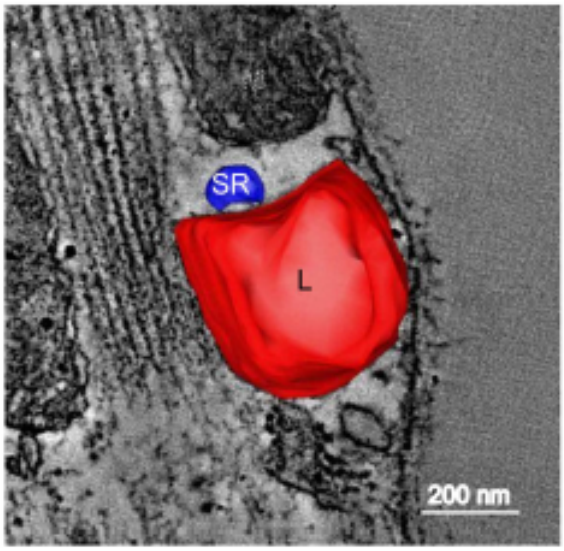


Department of Mathematics
Faculty of Sciences

VU UNIVERSITY AMSTERDAM

# Abstract

In this bachelor thesis we try and update the model from [Morotti et al., 2014] with recently found experimental data from [Capel et al., 2015] and [Aston et al., 2017]. The model in [Morotti et al., 2014] revolved around the excitability of a myocardiocyte and the modeling of the calcium ($Ca^{2+}$) currents during this excitability. Experimental data suggests that the lysosome has influence on these $Ca^{2+}$ currents. Because the model in [Morotti et al., 2014] does not include the lysosome, we will try and model the lysosomal $Ca^{2+}$ current into this model to get a better understanding of the influence on the mathematical problem. Our goal is to theoretically reproduce two of the experimental data-sets from [Capel et al., 2015]. To encounter this problem, we first need to understand how these currents are modeled. After specifying these currents and modeling of different channel- and receptor-mediated currents, we state our constructed models including parameters. We give the results of these models, discuss them and compare them to the model from [Morotti et al., 2014] and to the experimental data from [Capel et al., 2015]. We conclude that the models works in the long run, but still needs some optimization. Therefore, we suggest that a newer model must be used for further investigation on these $Ca^{2+}$ currents. Finally we state this model, and what assumptions have to be made to be sufficient to model the current knowledge of $Ca^{2+}$ currents.



Title: Mathematical modeling of ventricular fibrillation via calcium overload
Author: Erik Bosch, e.h.bosch@student.vu.nl,2539720
Supervisor: dr. Bob Planqué
Date: July 1, 2017

Department of Mathematics
VU University Amsterdam
de Boelelaan 1081, 1081 HV Amsterdam
`http://www.math.vu.nl/`

# Contents

# 1 Biomedical Introduction

## 1.1 How does the heart work?

The heart is essential for mammals as it pumps the blood through the vessels throughout the body. The blood works as a pathway for necessary substances such as nutrients and oxygen to be transported to the organs and transport waste products away from the organs such as carbon-dioxide ($CO_2$) and even heat. The heart is the driving force that keeps this process going. When the heart stops pumping blood through the body, waste product accumulates in the organs and in particular cells which causes malfunction and can result in death.
The pumping of the heart is caused by contraction of specific heart cells (myocardiocytes) in a specific order. This process is known as the cardiac cycle. The cardiac cycle revolves around two compartments: the atria and the ventricles. The atria and the ventricles are itself classified by their position in the heart as "left" or "right". The right atrium and the right ventricle are in the right part of the body and are responsible for pumping the blood to the lungs and back to the heart, this is called the pulmonary circulation. The pulmonary circulation carries deoxygenated blood away from the heart, to the lungs, and returns oxygenated blood back to the heart. The left atrium and left ventricle are responsible for pumping the blood to the other organs and back to the heart, this is called the systemic circulation. The systemic circulation carries oxygenated blood away from the heart to all parts of the body except the lungs and carries deoxygenated blood back to the heart.

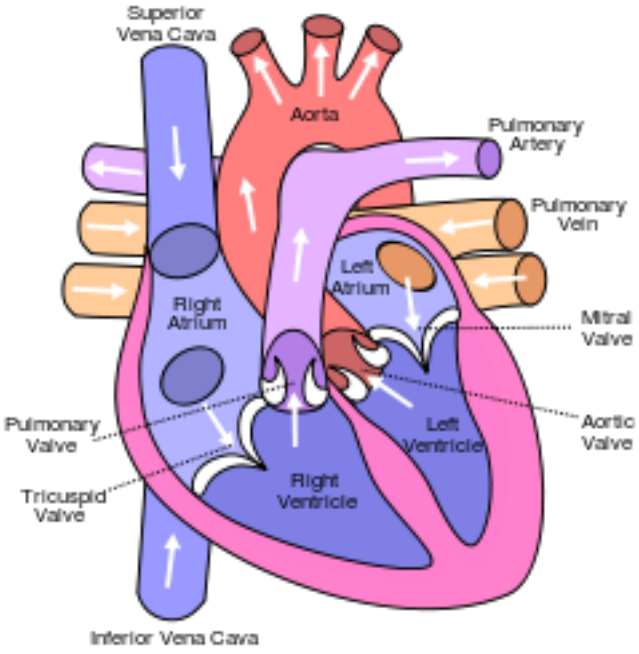


Figure 1.1: Schematic overview of the heart and how components of the heart are called.

The cardiac cycle begins with an electric pulse which is generated in the so called sinoatrial node (SN) located in the upper wall of the right atrium. This causes the atria to contract, raising the pressure in the atrium to such a level that it is higher than the pressure in the ventricles. The pressure difference is needed such that the atrioventricular (AV) valves open and blood flows into the ventricles. As blood flows into the ventricles, the atria pressure lowers until the pressure is again lower than the ventricle pressure. This causes the AV valves to close again. The electric pulse now reaches both the ventricles causing them to contract. Ventricle pressure is raised until this pressure is higher than the pressure in the pulmonary artery for the right ventricle and higher than the pressure in the aorta for the left ventricle (see Figure (1.1)). When this pressure level has been overcome, the blood is pushed into the pulmonary artery and into the aorta and starts to flow to the organs. During this process, the atria started to fill with blood such that another electrical pulse can start the cardiac cycle again. Thus, the pressure is essential for the working of the heart to pump the blood around.
An electrocardiogram (ECG) can measure the voltage through the heart as it beats. Each part in the ECG has its own label and corresponds to activation of the atria or the ventricles. The P-wave represents the activation of the atria. The QRS-complex represents the activation of the ventricles in downwards direction while the S-wave represents the activation of the ventricles but in upwards direction (see Figure (1.2)). For a normal patient the ECG has a characteristic sinus wave with the PQRST-tops visible. Medical conditions involving the heart are partly diagnosed by interpreting the ECG of the patient.

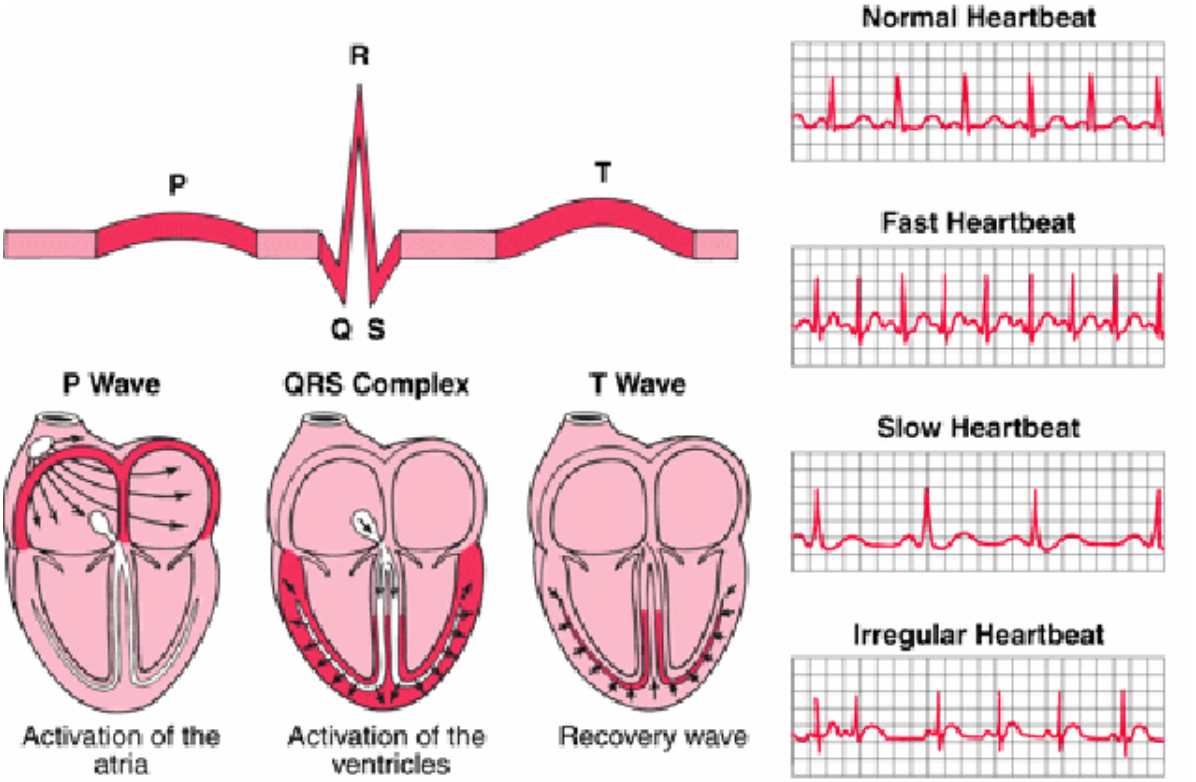


Figure 1.2: Schematic overview of the cardiac cyle.

## 1.2 How do myocardiocytes work?

The contraction of the myocardiocytes gives rise to higher pressure in the atria or the ventricles. The contraction of a myocardiocyte is caused by a series of processes within the myocardiocyte itself. The electrical pulse is passed from one myocardiocyte to another via an cardiac action potential. This cardiac action potential has five phases based on the flux of ions in and out of the myocardiocyte. The cardiac action potential follows a certain pattern, which we will describe here.

- Phase 4: the myocardiocyte is in resting state, with a membrane potential of -90 mV.
- Phase 0: so called quick-sodium-channels (QSC) open, such that sodium ($Na^+$) flows into the myocardiocyte making the membrane potential about +50 mV. This is called depolariation.
- Phase 1: the QSC close such the flow of $Na^+$ into the myocardiocyte is terminated while potassium ($K^+$) channels briefly open such that $K^+$ flows out of the myocardiocyte.
- Phase 2: $K^+$ still flows out of the cell while a flow through the so called L-type $Ca^{2+}$ channels of calcium ($Ca^{2+}$) into the myocardiocyte starts. This flow

of $Ca^{2+}$into the myocardiocyte not only causes the contraction of the myocardiocyte but also activates chloride ($Cl^-$) channels. These channels allow $Cl^-$ to enter the myocardiocyte.

- Phase 3: the L-type $Ca^{2+}$ channels close while $K^+$ channels remain open. These remain open until the membrane potential is restored to -90 mV. This is called repolarisation.

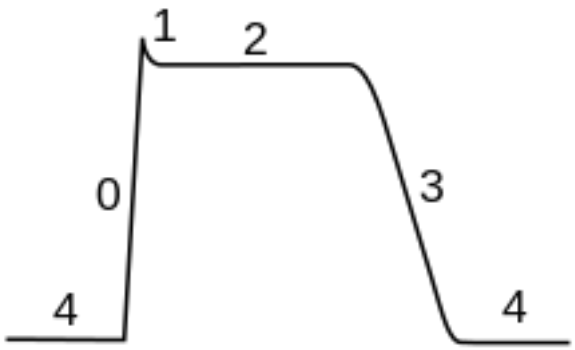


Figure 1.3: Schematic overview of the phases of a cardiac action potential.

## 1.3 Ventricular fibrillation

Ventricular fibrillation is a medical condition involving the myocardiocytes. As we have seen previously, the ventricles have to produce pressure to pump the blood. The myocardiocytes contract at the same time. A patient with ventricular fibrillation does have myocardiocytes that contract, but not at the same time. This results into failure of the ventricles to pump the blood around the body effectively. This is a major risk for the patient and can cause death. Ventricular fibrillation thus stands for the disorganized pumping of the heart. This can be seen in the ECG of a patient where most of the time the amplitude of the PQRST-tops are smaller than normal. The disorganized pumping of the heart can also have another cause, which we will discuss in the next subsection.

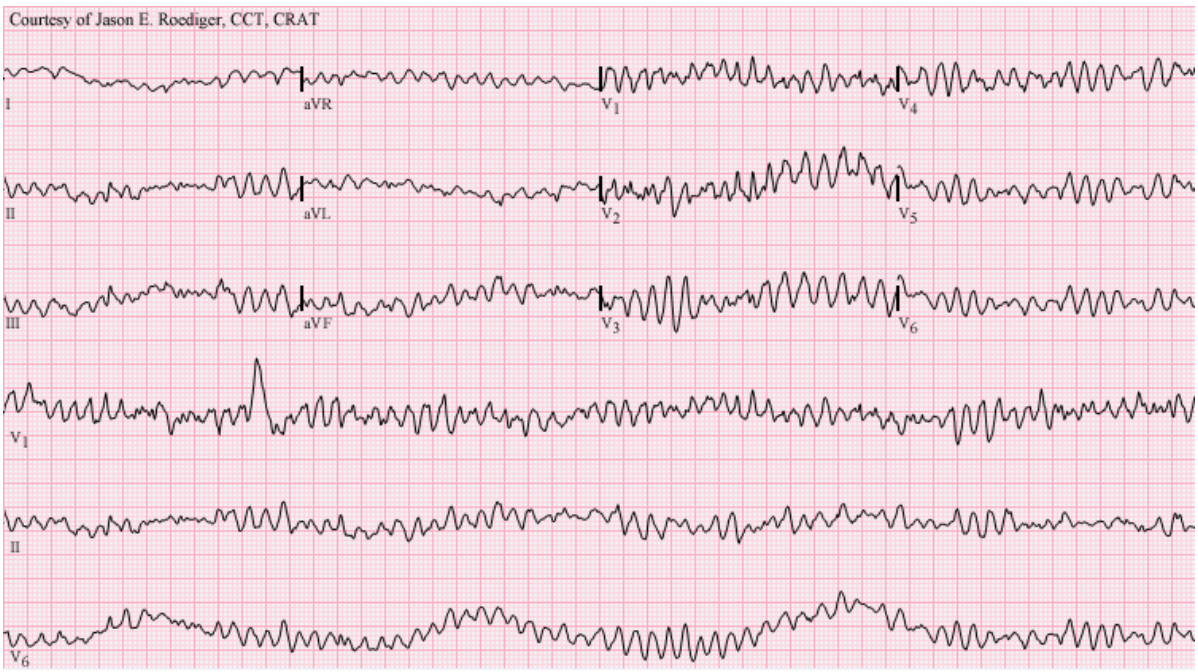


Figure 1.4: Ventricular fibrillation can be diagnosed by interpreting the ECG of a patient.

## 1.4 The role of $Ca^{2+}$ in the myocardiocytes

It is known that $Ca^{2+}$ has an important role in the myocardiocytes. During action potential phase 2 mentioned before leads the influx of $Ca^{2+}$ to a so called Calcium-induced calcium release (CICR). This means that the little influx of extracelluair-$Ca^{2+}$ into the cytosol of the myocardiocyte induces a bigger influx of intracellulair-$Ca^{2+}$ into the cytosol. The bigger influx of $Ca^{2+}$ comes out of the Sarcoplasmic Reticulum (SR), an organel in the cytosol of the myocardiocyte, which stores massive amounts of $Ca^{2+}$compared with the cytosol. The result of this bigger influx into the cytosol is that the myofilaments, the fibers that perform the actual physical contraction, are activated, as the threshold of $Ca^{2+}$ is reached.
Thus, the small influx of $Ca^{2+}$ leads to a physical contraction, or in other words, a small change in the concentration gradient of $Ca^{2+}$ in the cytosol leads to a physical contraction. Therefor, the concentration of $Ca^{2+}$ in the myocardiocyte should always be closely regulated. The disorganised pumping of the heart seems to be a result of an unwanted influx of $Ca^{2+}$ into the cytosol. We will describe in the next section what a reason could be of unwanted influx of $Ca^{2+}$ and thus unintentional contraction which causes ventricular fibrillation.

## 1.5 Involvement of the lysosome in ventricular fibrillation

The lysosome is an membrane-bound organelle found in every animal cell. Because of its membrane it can engulf all sort of biomolecules, such as peptides, nucleic acids, carbohydrates and lipids. The internal cytosol of the lysosome is called the lumen. The lumen contains a variety amount of enzymes, such that it can break down all biomolecules it engulfs. It is known that the lumen also contains a great storage of $Ca^{2+}$, just like the SR. It has been proposed that the lysosome plays a part in ventricular fibrillation [Capel et al., 2015] because there seems to be an influx of $Ca^{2+}$ into the cytosol, originated from the lysosome. This relies on the activation of molecules that are integrated into the lysosome membrane, the so called $Ca^{2+}$-permeable type 2 Two-pore channels (TPC). The activation of TPC is caused by a widely used messenger-molecule called Nicotine Acid Adenine Dinucleotide Phosphate (NAADP) that binds to the TPC. It has been found that the TPC is essential for a NAADP-induced lysosomal-$Ca^{2+}$ influx [Capel et al., 2015].

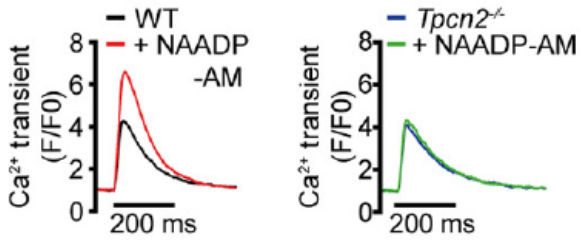


Figure 1.5: Shows superimposed $Ca^{2+}$ transients in myocardiocytes before and after application of NAADP-AM (240 nM) from [Capel et al., 2015].

This has been tested by [Capel et al., 2015] who used a membrane-permeant acetoxymethyl ester of NAADP called NAADP-AM to stimulate both wild-type (WT) mice myocardiocytes and modified mouse myocardiocytes which did not have working TPCs. The latter are called TPC-knockout mice. These tests were performed and showed that when NAADP-AM was used to stimulate WT mice, the amplitude of $Ca^{2+}$ transient was significantly increased, while NAADP-AM failed to increase the $Ca^{2+}$ transient in TPC-knockout mice. This can be seen in Figure (1.5).

Our main goal is to see if we can make a mathematical model that can reproduce these curves. We will extend the mathematical model given in [Morotti et al., 2014] with information from [Capel et al., 2015] and [Aston et al., 2017]. This extension will revolve around the addition of the lysosome and NAADP dependent lysosomal $Ca^{2+}$ current that has been experimentally observed, like in [Aston et al., 2017] and Figure (1.6). Experimental data suggested that the lysosome interacts in close range with the SR see Figure (1.7) .

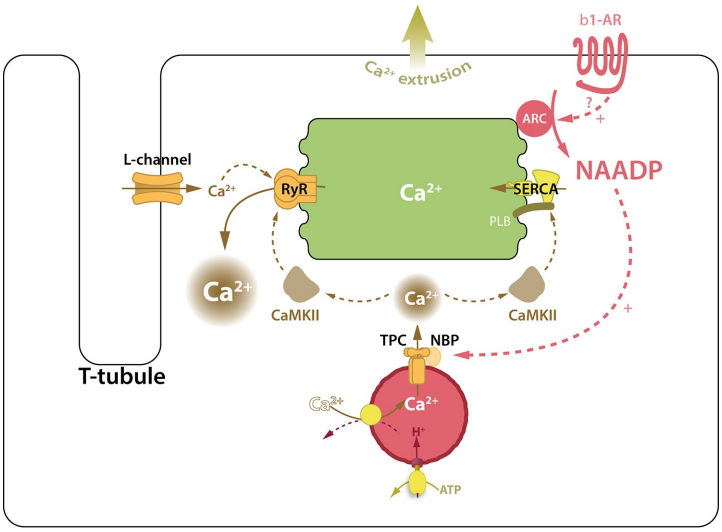


Figure 1.6: The model of [Capel et al., 2015] that suggests positive NAADP influences on TPC-$Ca^{2+}$ currents.

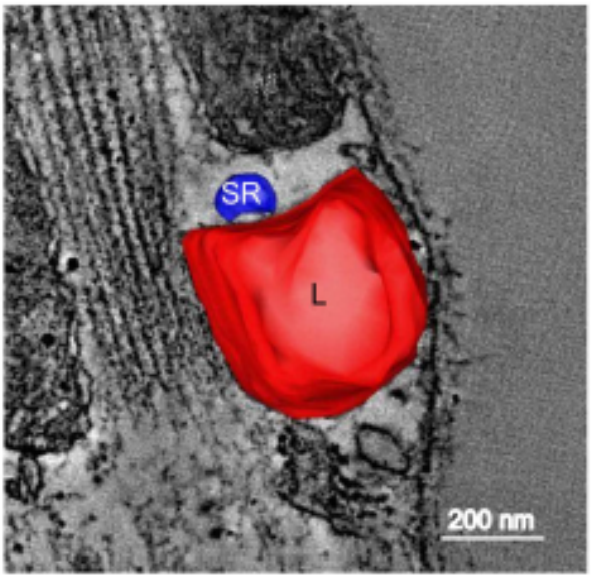


Figure 1.7: 3D Electron Tomography reconstruction of rabbit ventricular myocardiocytes, from [Aston et al., 2017].

# 2 Mathematical Introduction

## 2.1 Modeling of the cell membrane

The models of Alan Hodgkin and Andrew Huxley form the basis of all currently used mathematical models of electrophysiology of the heart or neuronal cells. They modeled the excitable cell as an electrical circuit, giving each component an electrical element. Charged ions account mostly for the signaling in and around the cell. Currents of these ions can be used to determine change of voltage. These currents are mostly mediated by channels and receptors. Because these also depend on the voltage itself, we will get a differential equation for voltage.

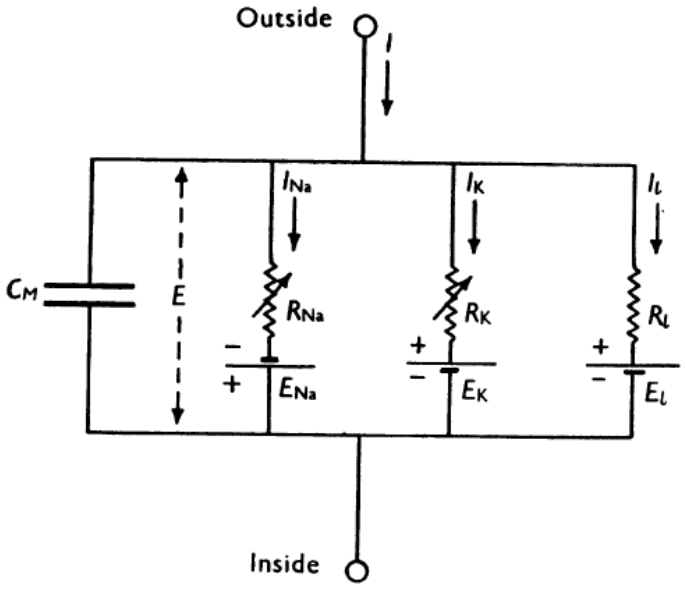


Figure 2.1: Electrical circuit representing the membrane.

Back to the model, the Hodgkin-Huxley model interprets the lipid layer as a capacitance ($C_m$, a constant), Voltage-gated ion channels as electrical conductances ($g_n$, where the $n$ stands for the specific ion channel and $g_n$ is dependent of voltage and time), as well as for the Leak channels in the cell membrane ($g_L$). The Leak-channels (and the Leak-current accordingly) stand for all the channels (and currents accordingly) apart from $Na^+$ and $K^+$, because the currents of all the other ions are in this model are small. Hodgkin & Huxley also defined the difference between the membrane potential ($E$) and the potential for the $Na^+$ ions ($E_{Na}$). From the Coulomb's law and the observation that

the capacitance is defined as the ratio of the charge across the capacitor to the voltage potential necessary to hold that charge, thus $C_M = Q/V$, we get that the capacitance current $I_c = \frac{dQ}{dt} = C_M \frac{dV}{dt}$. There is also an ionic current in the cell. Assumed is that there is no buildup of charge on either the out- and the inside of the cell. Therefore, the sum of both the capacitance current and the ionic current should be zero, leading to Equation (2.1).

$$I = I_c + I_i = C_M \frac{dV}{dt} + I_i = 0 \tag{2.1}$$

where

- $I$ is the total membrane current density;
- $I_c$ is the capacitance current;
- $I_i$ is the ionic current density;
- $V$ is the displacement of the membrane potential from its resting value;
- $C_M$ is the membrane capacity per unit area;
- $t$ is time.

The next step is to divide the ionic current into the sum of $Na^+$, $K^+$ and Leak currents, thus

$$I_i = I_{Na} + I_K + I_L$$

Hodgkin & Huxley then continued to reason by using the Nerst-equation that the ion specific current is in linear form of

$$\begin{aligned} I_{Na} &= g_{Na}(V - V_{Na}), \\ I_K &= g_K(V - V_K), \\ I_L &= g_L(V - V_L). \end{aligned}$$

Each ionic conductance can be expressed in terms of a ion-specific constant times ion-specific functions to the power an ion-specific integer estimated to fit the best to experimental data where this ion-specific function is determined by a differential equation. These formulas are given in the following subsections.

### 2.1.1 The potassium conductance: $g_K$

First thing Hodgkin & Huxley did was describing $g_K$. They assumed that $g_K$ would obey to a differential equation dependent on voltage and time:

$$\frac{dg_K}{dt} = f(v, t).$$

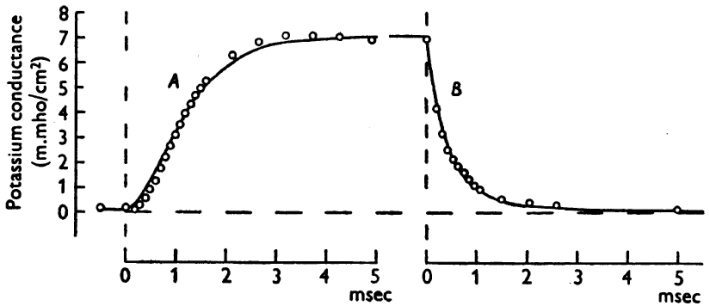


Figure 2.2: Experimental data from [Hodgkin and Huxley, 1952] for the pottassium conductance in a long giant squid axon from a squid nerve cell.

To fit the experimental data (see Figure (2.2)) that increased sigmoidal and decreased exponential, Hodgkin & Huxley reasoned that the potassium conductance should satisfy the formula

$$g_K = \bar{g_K} n^4, \tag{2.2}$$

where the fourth power was chosen to obtain the smallest error to fit to the experimental data in Figure (2.2) and $\bar{g}$ is some constant. The $n$ function in Equation (2.2) satisfies the differential equation

$$\tau_n(v)\frac{dn}{dt} = n_\infty(v) - n, \tag{2.3}$$

where $n_\infty(v)$ and $\tau_n(v)$ are defined as

$$n_\infty(v) = \frac{\alpha_n(v)}{\alpha_n(v) + \beta_n(v)}, \tag{2.4}$$

$$\tau_n(v) = \frac{1}{\alpha_n(v) + \beta_n(v)}. \tag{2.5}$$

To solve this differential equation, Hodgkin & Huxley opposed some (boundary) conditions, namely

- At $t = 0$, $v$ was elevated from 0 to $v_0$ and after that held constant.
- $n$ is at steady state when $t = 0$, i.e, $n(0) = n_\infty(0)$
- $n_\infty = 0$

Solving Differential Equation (2.3) with these conditions gives

$$n(t) = n_\infty(v_0)[1 - e^{-t/\tau_n(v_0)}], \tag{2.6}$$

which should be powered to the fourth to fit the sigmodial increasing. To fit the exponential decreasing, Hodgkin & Huxley solved Differential Equation (2.3) as

$$n(t) = n_\infty(v_0)e^{-t/\tau_n(0)}, \tag{2.7}$$

where again $n$ had to be powered to the fourth.
For any given voltage step, the time step $\tau_n$ and the final value of $n$, namely $n_\infty$, can be determined by fitting Equation (2.6) to the experimental data. After experimenting with many voltages, Hodgkin & Huxley fitted a continuous functions for $n_\infty$ and for $\tau_n$ in Equations (2.4) and (2.5) respectively to the discrete data-sets. Fitting of these functions have even lead to exact descriptions for $\alpha_n(v)$ and $\beta_n(v)$ as in Equation (2.4).

### 2.1.2 The sodium conductance: $g_{Na}$

Hodgkin & Huxley used for the sodium conductance with the same method which they used for the potassium conductance, although the sodium conductance seemed more complex. The equation should not only take account for the activation of the $Na^+$ current, but also inactivate the $Na^+$ current. Because of this, Hodgkin & Huxley reasoned that the equation for potassium conductance $g_{Na}$ would be

$$g_{Na} = g_{\bar{Na}} m^3 h,$$

with $m$ and $h$ obeying the same equation as $n$ in Differential Equation (2.3), with their own voltage dependent functions. The function $m$ activates the $Na^+$ current, while $h$ inactivates the $Na^+$ current. Again by fitting to experimental data, one can obtain continuous functions for these discrete data-sets.

## 2.2 Modeling of flux in the cell through compartments

Mathematical modeling of a cell is done through compartments. We treat each organelle as a compartment with its own characteristics. The more compartments, the more can be taken into account and that makes the model closer to reality. But more compartments does give rise to more variables which makes the model harder to interpret. The compartment model used in [Morotti et al., 2014] can be seen in Figure (2.3)

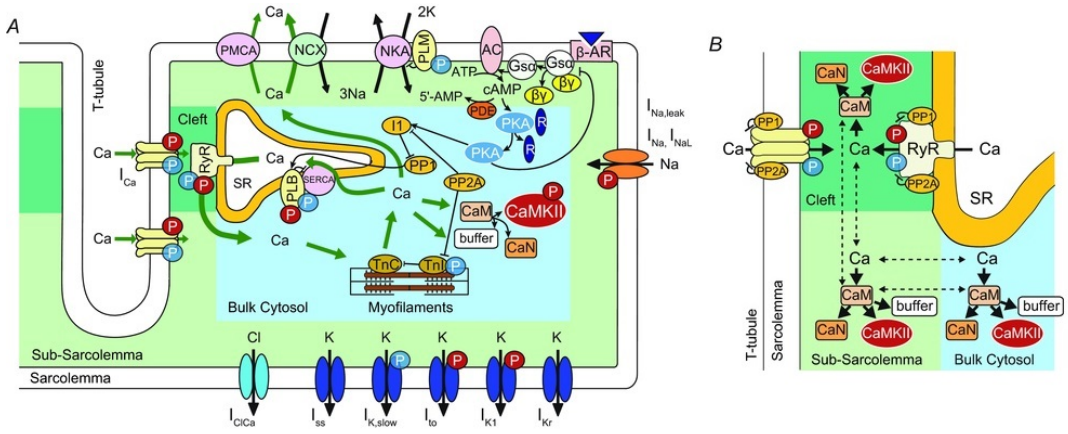


Figure 2.3: The model with interactions suggested in [Morotti et al., 2014].

We have seen in Section (2.1) that the cell membrane can be modeled as one compartment of the cell. Other compartments that we look at are the SR, the Cytosol, the Sarcolemma (SL), the Bulk-Sarcolemma and the Lysosome. Although there are around 50 to 1000 lysosomes in mammalian cells with different sizes, we define the Lysosome-compartment as only one lysosome with specific characteristics. The same modeling thought accounts for the SR. The cytosol of the cell is a fluid where proteins and other substances are dissolved and all organelles are in contact with. That is a reason to treat the cytosol as well as a compartment of the cell.
Statistical data suggest that some organelles do have certain affinity to specific places in the cytosol [Capel et al., 2015]. Electron microscopy showed that tight gaps are formed between the lysosome and the SR and between the sarcolemma and the SR as well. We call these tight gaps between organelles junctions. Because the model utilizes concentration of ions, concentrations can differ in these junctions as the volume of a junction is significantly less than the Cytosol. We model these junctions separate of the cytosol, for this reason. Because physically the Junction and Cytosol compartments consist of the same fluid there is diffusion between them. One more reason of separating the Cytosol compartment is that a small difference of concentration in the Junction compartment causes an bigger flux in the Junction compartment compared to the Cytosol compartment because of the bigger volume of the Cytosol compartment. This is important because some ion-channels are activated through difference of concentration in their neighborhood of a certain substance, which we will discuss in the next subsection. A widely used term for this event is that the the ion-channel has a specific activating threshold.
To describe the interaction between such compartments we will explain an adaption of a model used in [Penny et al., 2014], which we will use for our models. We define the compartments as followed: the Cytosol, the Junction, the Lysosome and the Endoplasmic Reticulum (ER). Because the ER and the SR have common characteristics we can use this model for our own model. Their model was based around the $Ca^{2+}$ flux between these compartments. The Cytosol and the Junction consist as previously explained of the same fluid, and therefore there is some diffusion of $Ca^{2+}$ between these compart-

ments. In general is flux given by the symbol $J$ and is sometimes through a membrane. When this is the case, a mediator molecule is used to pass through this membrane. The mediators that we model are the TPC, the inositol triphosphate receptor (IPR) and the Sarco/endoplasmic reticulum $Ca^{2+}$-ATPase (SERCA). The mediators are somewhat modeled differently, which we will discuss in the next section.

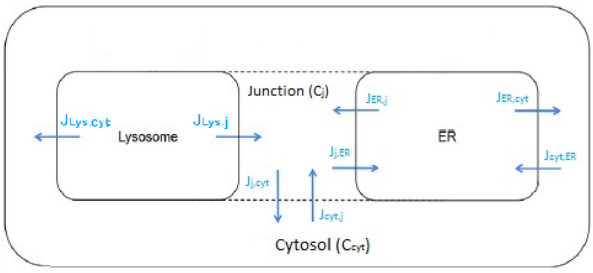


Figure 2.4: Adaption of the model in [Penny et al., 2014].

| Flux | From | To | Mediator |
|---|---|---|---|
| $J_{j,cyt}$ | Junction | Cytosol | None |
| $J_{cyt,j}$ | Cytosol | Junction | None |
| $J_{l,j}$ | Lysosome | Junction | TPC |
| $J_{l,cyt}$ | Lysosome | Cytosol | TPC |
| $J_{ER,j}$ | ER | Junction | IPR |
| $J_{ER,cyt}$ | ER | Cytosol | IPR |
| $J_{j,ER}$ | Junction | ER | SERCA |
| $J_{cyt,ER}$ | Cytosol | ER | SERCA |

Table 2.1: Table of the flux variables and its mediators.

These fluxes are then modeled by the following equations:

$$
\begin{aligned}
J_{j,cyt} &= D_C(C_j - C_{cyt}),\\
J_{cyt,j} &= D_C(C_{cyt} - C_j),\\
J_{l,j} &= k_t P_{oTPC}(C_l - C_j),\\
J_{l,cyt} &= k_t P_{oTPC}(C_l - C_{cyt}),\\
J_{ER,j} &= k_{IPR} P_{oIPR}(C_{ER} - C_j),\\
J_{ER,cyt} &= k_{IPR} P_{oIPR}(C_{ER} - C_{cyt}),\\
J_{j,ER} &= \frac{V_{SERCA} C_j^{1.75}}{K_{SERCA}^{1.75} + C_j^{1.75}},\\
J_{cyt,ER} &= \frac{V_{SERCA} C_{cyt}^{1.75}}{K_{SERCA}^{1.75} + C_{cyt}^{1.75}},
\end{aligned}
$$

where $D_C$ is a diffusion- or rate-constant for $Ca^{2+}$ in the cytosol and parameters $k$ are rate-constants related to the density of the specific ion-channels. The term $P_{oTPC}$ is the

fraction of TPCs that are activated and open, this term is modeled in Section (2.3). The concentration of lysosomal $Ca^{2+}$ ($C_l$) and the concentration of ER-$Ca^{2+}$ ($C_{ER}$) are assumed constant and therefore no differential equations will be modeled for these concentrations. All the fluxes have unit concentration over time.
Assuming no flux across the cell membrane, we get the following differential equations for $C_{cyt}$:

$$\frac{dC_{cyt}}{dt} = J_{ER,cyt} + J_{l,cyt} - J_{cyt,ER} + J_{j,cyt}.$$

For the equation of Junction $Ca^{2+}$ , the fact that the volume of the Junction is different from the volume of the Cytosol has to be taken into account. This leads to the differential equation for $C_j$ to be

$$\frac{dC_j}{dt} = R_V J_{ER,j} + R_V J_{l,j} - R_V J_{j,ER} + R_V J_{cyt,j}.$$

The parameter $R_V$ represents the ratio of the volumes of the compartments $R_V = \frac{V_{Cyt}}{V_j}$.

## 2.3 Modeling of ion mediator in the organelles

We encountered in the previous subsection three different ion mediators: the TPC, the IPR and the SERCA. The flux via these big mediators can be mathematically modeled in different ways. We will discuss both models for these mediators.

### 2.3.1 Modeling of the TPC and the IPR

Because the TPC and the IPR are modeled the same way we will only work out the model for the TPC. We begin with assuming that the TPC has two ports, but only that the TPC is open when both of these are activated.
We assume that these ports switch independently of each other between open and closed. We define a binary counter that tells us in what state the port is, whether a port is activated or not, and also define $X$ as the TPC as whole. $X_{11}$ thus means that both ports are activated and the TPC is open, while $X_{01}$ means that the first port is activated and the second is not which means the TPC is not open. Because there is no biological difference between $X_{01}$ and $X_{10}$ we can define a new variable $H$ that represents the TPC with a counter that tells us how many ports are activated. The TPC switches from one combination of states to another with some rate. We define these rates $\alpha$ when a port is activated and $\beta$ when a port is deactivated.
Because we are more interested in the fraction of TPCs that are open, and not the amount, we normalize each variable $H$ with the total amount of $H$ and define this the variable $S$: $S_i = \frac{H_i}{H_{tot}}$ for $i = \{0, 1, 2\}$. Obviously because of our definition of $S$ we have that $S_0 + S_1 + S_2 = 1$. The chemical reaction scheme then looks like this:

$$S_0 \underset{\beta}{\overset{2\alpha}{\rightleftarrows}} S_1 \underset{2\beta}{\overset{\alpha}{\rightleftarrows}} S_2.$$

This gives rise to the three differential equations for $S_0$, $S_1$ and $S_2$. Because of $S_0 + S_1 + S_2 = 1$ we can drop the differential equation for $S_1$. We will only have to look at differential equations for $S_0$ and $S_2$:

$$\begin{aligned} \frac{dS_0}{dt} &= \beta S_1 - 2\alpha S_0, \\ \frac{dS_2}{dt} &= \alpha S_1 - 2\beta S_2. \end{aligned} \tag{2.8}$$

What determines the flux from the Lysosome through the TPC to the Junction? This flux is dependent of the difference of $C_l$ and $C_j$ and of the rate $k_t$ but this assumes that the TPC is open all the time. This is certainly not true. Differential equation (2.8) says that the fraction of TPC that is open, changes over time. Thus, $S_2$, the fraction of TPCs that is open has influence on the flux through the TPC. We call the factor $S_2$ the open probability for TPC and is denoted by $P_{oTPC}$. This leads to the flux from the Lysosome through the TPC to the Junction to be

$$J_{l,j} = k_t P_{oTPC}(C_l - C_j). \tag{2.9}$$

This model can be extended for channels that have for example more ports and even a new variable that determines whether a port is activated or not. The IPR model makes use of three equivalent and independent ports. Each port has three different properties that can determine its state. The first is an $IP_3$ binding site, which is the activator of the IPR. Second is an activating $Ca^{2+}$ binding site and an $Ca^{2+}$ inactivating binding site. Therefor each port can be labeled as $H_{ijk}$ where $i, j, k$ indicate the properties previously and have either value 0 for unoccupied and 1 for occupied. Once again we can make a new $S$ variable for the fraction of total IPRs, and write down the differential equations for those. Experimental data indicates that each port works cooperative, which means for the $Ca^{2+}$ current that when all three ports is in state $S_{110}$, $Ca^{2+}$ flux is possible. Because each port is independent of each other, the open probability of IPR is $P_{oIPR} = S_{110}^3$.

### 2.3.2 Modeling of the SERCA

The model for the SERCA uses another base model. We start with a model that describes the interaction of an enzyme with two substrate molecules. The enzyme can exist in unbounded, bounded with one molecule of substrate and bounded with two molecules of substrate. The complex of enzyme and substrate(s) can degrade into the free enzyme and a product or the complex and a product. We define again the rates and thus the reaction chain looks like

$$S + E \underset{k_{-1}}{\overset{k_1}{\rightleftarrows}} C_1 \overset{k_2}{\to} E + P$$
$$S + C_1 \underset{k_{-3}}{\overset{k_3}{\rightleftarrows}} C_2 \overset{k_4}{\to} C_1 + P. \tag{2.10}$$

Determining this system gives five differential equations for $S$, $E$, $C_1$, $C_2$ and $P$. Because of the conservation of the amount of enzyme and the differential equation for P can be solved manually by integrating, we can decrease the model to three differential equations

$$\frac{dS}{dt} = -k_1SE + k_{-1}C_1 - k_3SC_1 + k_{-3}C_2,$$
$$\frac{dC_1}{dt} = k_1SE - (k_{-1} + k_2)C_1 - k_3SC_1 + (k_4 + k_{-3})C_2, \tag{2.11}$$
$$\frac{dC_2}{dt} = k_3SC_1 - (k_4 + k_{-3})C_2. \tag{2.12}$$

Next we set $\frac{dC_1}{dt}$ and $\frac{dC_2}{dt}$ both equal to zero. This has been proposed by Briggs & Haldane in 1925 who assumed that the rates of formation and breakdown of complexes are essentially equal at all times, disregarding the beginning of the reaction [Briggs and Haldane, 1992]. Thus, $\frac{dC_1}{dt} = 0 = \frac{dC_2}{dt}$. This method is called the quasi-steady-state approximation. Assuming the quasi-steady-state approximation and solving for $C_1$ and $C_2$ gives

$$C_1 = \frac{K_2E_0S}{K_1K_2 + K_2S + S^2},$$
$$C_2 = \frac{E_0S^2}{K_1K_2 + K_2S + S^2}, \tag{2.13}$$

where $K_1$,$K_2$ and $E_0$ are constants given by $K_1 = \frac{k_{-1}+k_2}{k_1}$, $K_2 = \frac{k_4+k_{-3}}{k_3}$ and $E_0 = E + C_1 + C_2$. This leads to the flux being

$$J = k_2C_1 + k_4C_2 = \frac{(k_2K_2 + k_4S)E_0S}{K_1K_2 + K_2S + S^2}.$$

Now we can put some conditions on the rate values: let us say that $k_1 \to 0$ and $k_3 \to \infty$ while keeping $k_1k_3$ constant. The biological meaning of this is that the enzyme and the first substrate bind very slowly, but when the complex is formed it immediately binds another substrate. This results into the flux being

$$J = \frac{k_4E_0S^2}{K_1K_2 + S^2} = \frac{V_{max}S^2}{K_m^2 + S^2},$$

where we define $V_{max} = k_4 E_0$ and $K_m^2 = K_1 K_2$. This basic model for one substrate can be extended to $n$ substrates under the condition that $k_1 \to 0$ and $k_n \to \infty$ while keeping $k_1 k_n$ constant, which gives

$$J = \frac{V_{max} S^n}{K_m^n + S^n}$$

where $K_m^n = \Pi_{i=1}^n K_i$. This $n$ is called the Hill-coefficient and can be found through experimental data. It is not unusual that the best fit for $n$ to be non-integer, which explains our value of $n = 1.75$ which has been suggested in [Pitt et al., 2010]. This leads to the flux being

$$\begin{aligned} J_{j,ER} &= \frac{V_{SERCA} C_j^{1.75}}{K_{SERCA}^{1.75} + C_j^{1.75}}, \\ J_{cyt,ER} &= \frac{V_{SERCA} C_{cyt}^{1.75}}{K_{SERCA}^{1.75} + C_{cyt}^{1.75}}, \end{aligned} \tag{2.14}$$

These fluxes are similar to the fluxes that will be used in the [Morotti et al., 2014] model, of course applied on the SR instead of the ER.

# 3 Our Models

The modeling of $Ca^{2+}$ flux in a myocardiocyte with a junction that is formed between the SR and the Sarcolemma was first done in 2004 [Shannon et al., 2004]. Over the years this model was extended with more compartments in it through several papers. A recent one was [Morotti et al., 2014], which we will be using as foundation of our models. All these papers used a computational model programmed in MatLab. All our models are based around the placement of the newly defined Lysosome compartment and the following lysosomal $Ca^{2+}$ current into the existing model of [Morotti et al., 2014]. For each model we define new differential equations and new parameters that are involved.

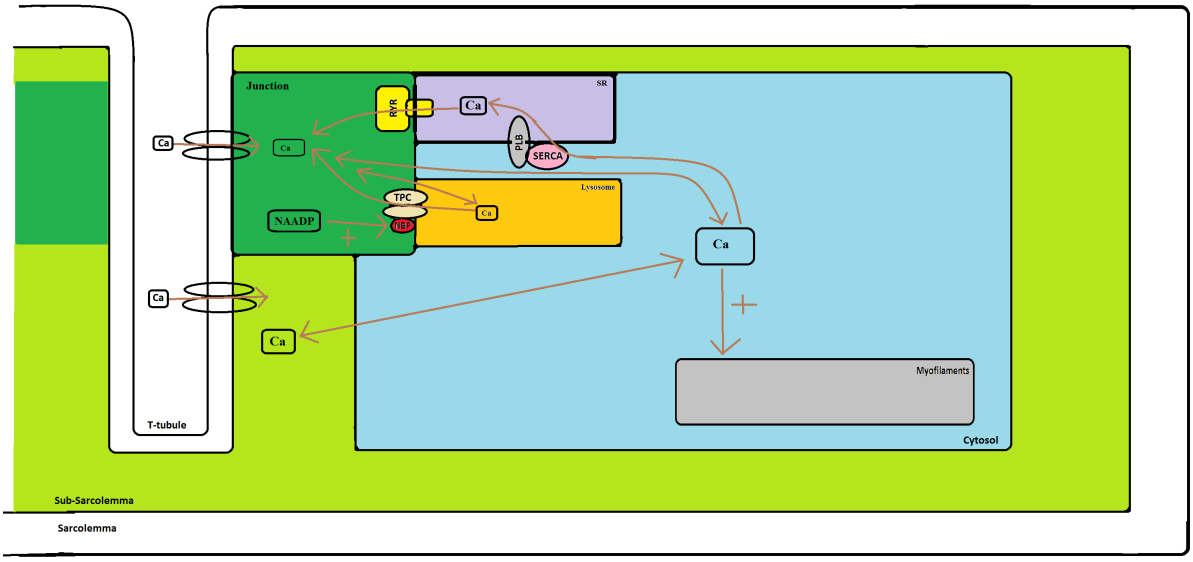


Figure 3.1: Schematic figure of Model 1 and 2, only changed parts compared with [Morotti et al., 2014] are shown.

Because the lysosome is a storage of $Ca^{2+}$ we will also model whether we keep the lysosomal $Ca^{2+}$ concentration fixed or variable. First of all we have to know some geometry of the lysosome to define our Lysosome compartment. We define the volume of the Lysosome compartment as in [Penny et al., 2014]. The call the parameter that determines the diffusionrate from $Ca^{2+}$ between the Junction and the Lysosome $D_C$ as found in [Allbritton et al., 1992]. We estimate the parameter that represents the rate of the flow from the Lysosome to the Junction $k_{Ls}$ by averaging $k_{Ls}$ values from Penny et al 2014 [Penny et al., 2014], Table 1. Next we define the concentration of NAADP, which we choose to fit to the experimental methods used in [Capel et al., 2015] and the open

probability of TPC $P_{oTPC}$. The relation between $P_{oTPC}$ and the NAADP was found to be bell-shaped. The optimum of $P_{oTPC}$ was 0.014 at 23 $nM$ NAADP as in [Pitt et al., 2010]. We choose, as in [de Jong, 2016], the standard deviation of this formula to be 1.5 such that it would fit the data of [Pitt et al., 2010].

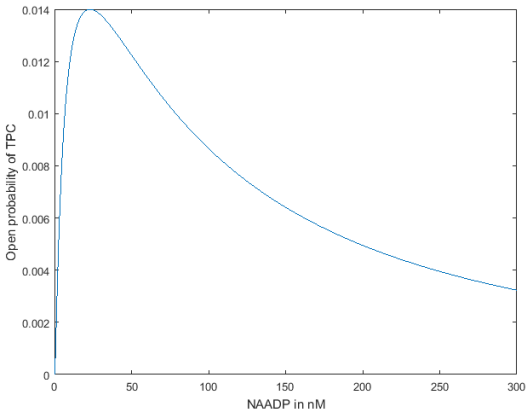


Figure 3.2: The bell-shaped relation between the openprobability of the TPC and the concentration of NAADP.

We define the rate of the flow of $Ca^{2+}$ through the TPC induced by NAADP $k_t$. We estimate this parameter by data of [Fameli et al., 2014], which says that a typical flow of CICR is about $300nM$ in $0.3ms$. This is equal to $1.0 \cdot 10^{-3} mM/ms$. Therefore we can estimate parameter$k_t$ using the formula $J_{mLs} = k_t P_{oTPC}(Ca_{Lys,init} - Ca_{j,init})$. We let the distance from the Lysosome to the Junction be $distLysjunc$ corresponding to the findings [Capel et al., 2015]. The parameter $D_{callysjunc}$ got the value of the average of the values of $D_{calSLcyto}$ and $D_{calJuncyto}$ in [Morotti et al., 2014]. Finally, we define the parameter $J_{ca,junclys}$ which we calculate with the same constructed formula as in [Morotti et al., 2014]. See for all values, units, formulas and sources Table (3.1).

| Parameters | Formula | Value | Unit |
|---|---|---|---|
| $V_{Lys}$ | $0.01^{(2)}V_{Cell}^{(1)}$ | $3.3006 \cdot 10^{-13}$ | $L$ |
| $k_{Ls}^{(0)}$ | $(k_{Ls}^{(2)} + k_{Ls}^{(2)})/2$ | $0.01125 \cdot 10^{-3}$ | $ms^{-1}$ |
| $J_{Ls}^{(0)}$ | $\Delta[Ca^{2+}]_{shoulder}^{(6)}/t^{(6)} \cdot 10^{-3}$ | $1.0 \cdot 10^{-3}$ | $mM/ms$ |
| NAADP$^{(3)}$ | - | 240 | $nM$ |
| $P_{oTPC}^{(5,7)}$ | $0.014 \cdot e^{-\frac{(log(NAADP)-log(23))^2}{2 \cdot 1.5^2}}$ | 0.004 | - |
| $k_t^{(0)}$ | $J_{mLs}^{(0,6)}/(Ca_{Lys,init}^{(1)} - Ca_{j,init}^{(1)})/P_{oTPC}$ | 0.4854 | $ms^{-1}$ |
| $\Delta_{Lys,junc}^{(3)}$ | - | $25 \cdot 10^{-3}$ | $\mu m$ |
| $D_C^{(4)}$ | - | $223 \cdot 10^{-3}$ | $\mu m^2/ms$ |
| $D_{callysjunc}^{(0)}$ | $(D_{calSLcyto}^{(1)} + D_{calJuncyto}^{(1)})/2$ | $1.34 \cdot 10^{-6}$ | $cm^2/s$ |

Table 3.1: Table of parameters for the Lysosome. (0): Our own method for estimating parameter. (1): Value from [Morotti et al., 2014]. (2): Value fitted to data of [Penny et al., 2014]. (3): Value from [Capel et al., 2015]. (4): Value from [Allbritton et al., 1992]. (5): Fitted to data of [Pitt et al., 2010]. (6): Value and method from [Fameli et al., 2014]. (7): Method from [de Jong, 2016].

## 3.1 Model 1: Lysosome - consisting compartment - fixed $Ca^{2+}$

In this model we define the Lysosome compartment and let it only interact with the Junction compartment that is modeled in [Morotti et al., 2014]. We assume that the Lysosomal $Ca^{2+}$ concentration does not change in time, which means it becomes a parameter and we define this parameter as $Ca_{Lys,init} = 0.5$ in unit $mM$ as in [Pitt et al., 2010]. We define the leak flux through the TPC between the Lysosome and the Junction like in [Penny et al., 2014] as $J_{mLsleak} = k_{Ls} \cdot (Ca_{Lys,init} - Ca_j)$ which has unit $mM/ms$. We also introduce the flux of Lysosomal $Ca^{2+}$ through the TPC into the Junction that is caused by NAADP like in [Penny et al., 2014]: $J_{mLs} = k_{Ls}P_{oTPC} \cdot (Ca_{Lys,init} - Ca_j)$ with unit $mM/ms$. This leads to a new differential equation for $Ca_j$

$$\begin{aligned}\frac{dCa_j}{dt} = &-\frac{1}{V_{junc}}\frac{C_{mem}}{2 \cdot Frdy}I_{Ca,tot,junc} + \frac{1}{V_{junc}}J_{ca,juncsl}(Ca_{sl} - Ca_j) - J_{CaB,junction} \\ &+ \frac{V_{sr}}{V_{junc}}J_{SRCarel} + \frac{V_{myo}}{V_{junc}}J_{SRleak} + \frac{V_{Lys}}{V_{junc}}J_{mLs} + \frac{V_{Lys}}{V_{junc}}J_{mLsleak} \\ &+ \frac{V_{Lys}}{V_{junc}}D_C J_{ca,junclys}(Ca_{Lys,init} - Ca_j),\end{aligned} \tag{3.1}$$

with unit $mM/ms$.

## 3.2 Model 2: Lysosome - consisting compartment - variable $Ca^{2+}$

In this model we define the Lysosome compartment and let it only interact with the Junction compartment that is modeled in [Morotti et al., 2014]. While we assumed in model 1 that the Lysosomal $Ca^{2+}$ concentration does not change in time, we will assume in model 2 that it does change in time. We conclude that we should compose a differential equation for $Ca_{Lys}$. This also means that the parameter $Ca_{Lys,init}$ in the flux equations described in model 1 should for model 2 be the variable $Ca_{Lys}$. The initial condition of it will still be $0.5mM$. We define the leak flux through the TPC between the Lysosome and the Junction as $J_{mLsleak} = k_{Ls} \cdot (Ca_{Lys} - Ca_j)$ which has unit $mM/ms$. We also introduce the flux of Lysosomal $Ca^{2+}$ through the TPC into the Junction that is caused by NAADP: $J_{mLs} = k_{Ls}P_{oTPC} \cdot (Ca_{Lys} - Ca_j)$ with unit $mM/ms$. Both definitions are again in line with the method in [Penny et al., 2014]. This leads to a new differential equation for $Ca_j$

$$\begin{aligned}\frac{dCa_j}{dt} = &-\frac{1}{V_{junc}}\frac{C_{mem}}{2 \cdot Frdy} I_{Ca,tot,junc} + \frac{1}{V_{junc}} J_{ca,juncsl}(Ca_{sl} - Ca_j) - J_{CaB,junction} \\ &+ \frac{V_{sr}}{V_{junc}} J_{SRCarel} + \frac{V_{myo}}{V_{junc}} J_{SRleak} + \frac{V_{Lys}}{V_{junc}} J_{mLs} + \frac{V_{Lys}}{V_{junc}} J_{mLsleak} \\ &+ \frac{V_{Lys}}{V_{junc}} D_C J_{ca,junclys}(Ca_{Lys} - Ca_j),\end{aligned} \tag{3.2}$$

with unit $mM/ms$.
To model the differential equation for $Ca_{Lys}$ we only need to specify the variable $I_{Ca,tot,Lys}$. We choose this variable to be zero because we could not determine from the the formulas how to define this this variable. Related variables were near zero but not did not have the same sign. Therefore we choose the variable to equal zero all the time, thus $I_{Ca,tot,Lys} = 0$. The total differential equating then followed to be

$$\begin{aligned}\frac{dCa_{Lys}}{dt} = &-\frac{1}{V_{Lys}}\frac{C_{mem}}{2 \cdot Frdy} I_{Ca,tot,Lys} - \frac{V_{junc}}{V_{Lys}} J_{mLsleak} - \frac{V_{junc}}{V_{Lys}} J_{mLs} \\ &+ \frac{V_{junc}}{V_{Lys}} D_C J_{ca,junclys}(Ca_j - Ca_{Lys})\end{aligned} \tag{3.3}$$

with unit $mM/ms$.

# 4 Results & Discussion

After numeric solving of the system, we made several plots for both the junction concentration $Ca_j$ and the cytosol concentration $Ca_{cyt}$ as well as the lysosomal concentration $Ca_{Lys}$ for model 2. The lysosomal concentration is a parameter for model 1 and therefor not important for comparing with the plots generated in [Capel et al., 2015], which we can see in Figure (4.1) and (4.2). Figure (4.1) shows the $Ca^{2+}$ transient in TPC-knockout myocardiocytes and TPC-knockout myocardiocytes stimulated with 240 $nM$ NAADP-AM.
In all experiments in [Capel et al., 2015] observation of $Ca^{2+}$ is done by a probe called Fluor-5F and makes use of fluorescence. When the cytosol $Ca^{2+}$ concentration raises, the fluorescence which is observed raises linearly as well. Therefor, fluorescence can describe the behavior of $Ca^{2+}$ concentration. They subtracted the background fluorescence of myocardiocytes from the changing fluorescence over time and is denoted $F$. This value $F$ is then scaled by the factor $F0$ which is the diastolic fluorescence value, such that the data is relative to the diastolic fluorescence for analytical reasons. This is the usual way of determining concentration differences over time. Because we do not have any fluorescence, obviously, we will be scaling the cytosol and junction $Ca^{2+}$ concentration with their own initial value concentrations. This way we get a plot that we can compare on overall behavior to the plots generated in [Capel et al., 2015].
Now we can state our results for each model. We have made plots for both $Ca^{2+}$ concentration with two different timescales: the first 5 seconds for overall behavior and then (timescale chosen by inspection) the first 0.05 seconds to obtain a closer look of the first period of the contraction. For comparing our results with the experimental data from [Capel et al., 2015], we adjust our timescale to 0.4 seconds, which resembles the

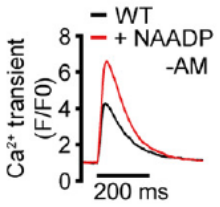


Figure 4.1: Shows $Ca^{2+}$ transient in Wild-type myocardiocytes and Wild-type myocardiocytes stimulated with 240 $nM$ NAADP-AM from [Capel et al., 2015].

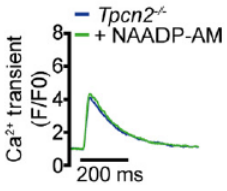


Figure 4.2: Shows $Ca^{2+}$ transient in TPC-knockout myocardiocytes and TPC-knockout myocardiocytes stimulated with 240 $nM$ NAADP-AM from [Capel et al., 2015].

data in [Capel et al., 2015], see Figure (4.1) and Figure (4.2).

## 4.1 Model 1

First observation is that the relative concentration of junction $Ca^{2+}$ and cytosol $Ca^{2+}$ behave very similar, but not enough to discuss only one. So we will discuss all plots for each concentration.

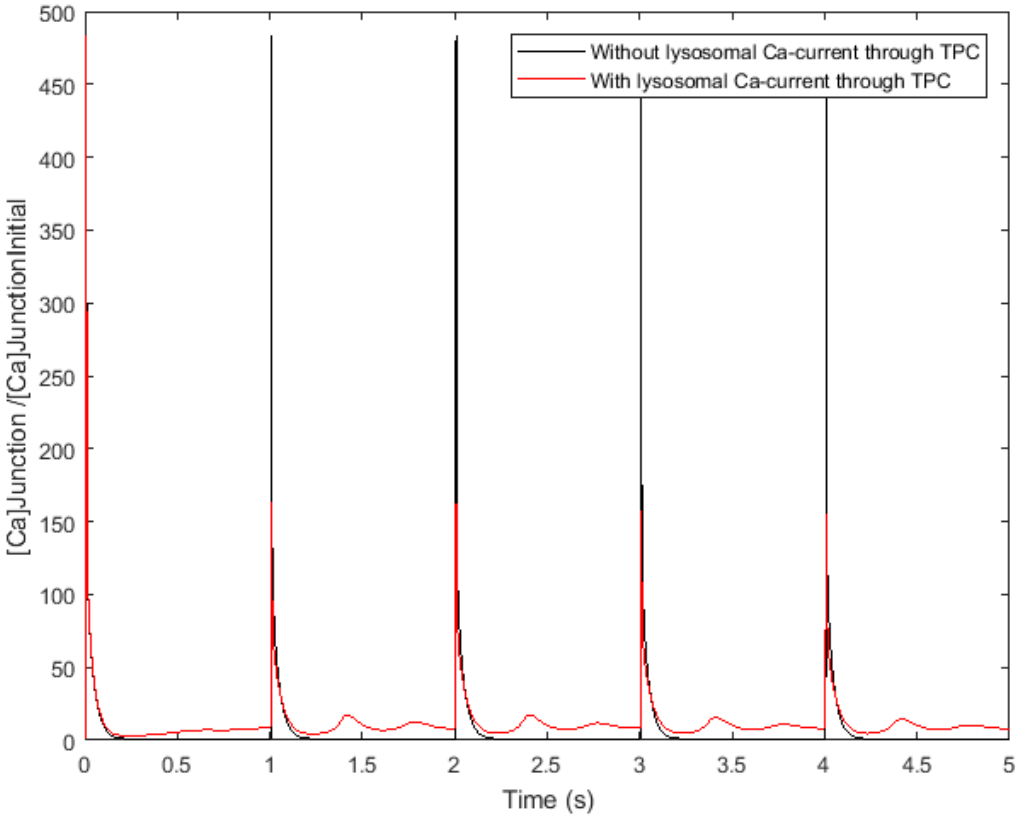


Figure 4.3: Results of comparing junction $Ca^{2+}$Wildtype myocardiocytes like in Morotti without lysosomal $Ca^{2+}$ current with junction $Ca^{2+}$ Wildtype myocardiocytes with lysosomal $Ca^{2+}$ current like in Model 1.

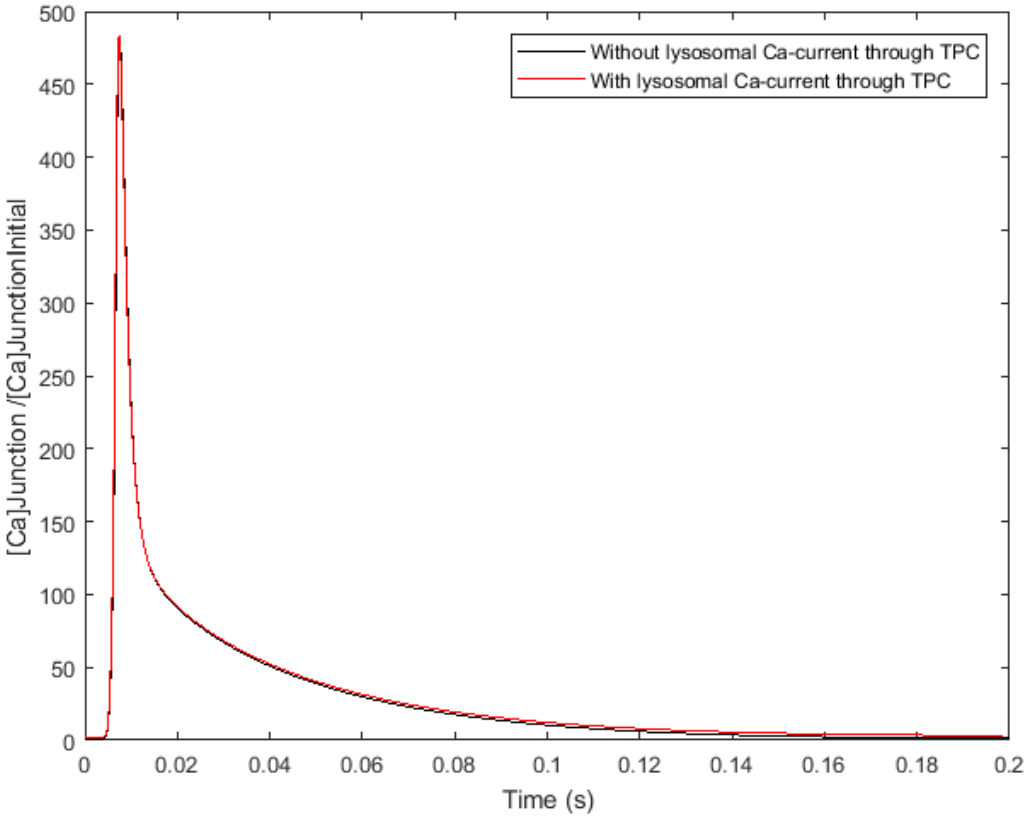


Figure 4.4: Results of comparing junction $Ca^{2+}$Wildtype myocardiocytes like in Morotti without lysosomal $Ca^{2+}$ current with junction $Ca^{2+}$ Wildtype myocardiocytes with lysosomal $Ca^{2+}$ current like in Model 1.

From Figure (4.3) we see that the results for both data-sets are closely the same until the time mark of 0.3 seconds and then diverge from each other. Both data-sets grow exponentially to an output peak of around 470 at the time mark of 0.01 seconds and then exponentially decay towards zero (see Figure (4.4)).
After this time mark, the lysosomal current data seems to decay more slowly, until at the time mark of 0.5 seconds this data-set starts to grow unregulated. The data that excludes the lysosomal $Ca^{2+}$ current still decays during this time interval. After each full second, a new peak is generated for both. The peaks differ from value significantly, with the data that includes lysosomal $Ca^{2+}$ current only reaching a consistent peak value of around 150 while the other data-set reaches consistent 470.
We can see that in the interval between the peaks the data that includes lysosomal $Ca^{2+}$ current behaves not like the other data-set. The data-set that includes lysosomal $Ca^{2+}$ current does exponentially decay but then generates in this interval two small normal-distribution-like tops with both tops at an output value of around 20 (see Figure (4.5)). This behavior continues in the next periodic intervals after the peak.
This might be because of the way we set the lysosomal $Ca^{2+}$ concentration and the open

probability of the TPC as parameters. Because these parameters do not change over time, this might result in an constant outwards flow of $Ca^{2+}$. We argue that the higher the concentration is in the junction compared with the lysosomal concentration, the less $Ca^{2+}$ will flow to the junction.
We described in Subsection (2.3.1) how the open probability of TPC can be modeled. This was not included on our mathematical model, as we used some earlier found results from [de Jong, 2016]. For further investigation, we can put this open probability in the mathematical model, or even extend this model further with activation and inactivation of open or closed ports. A suggestion might be that the activation of ports depends on the concentration of NAADP, but the switching of ports to open and closed state might depend on the $Ca^{2+}$ concentration. Therefore the open probability would not only depend on NAADP but also on the difference of $Ca^{2+}$ concentration in the compartments.

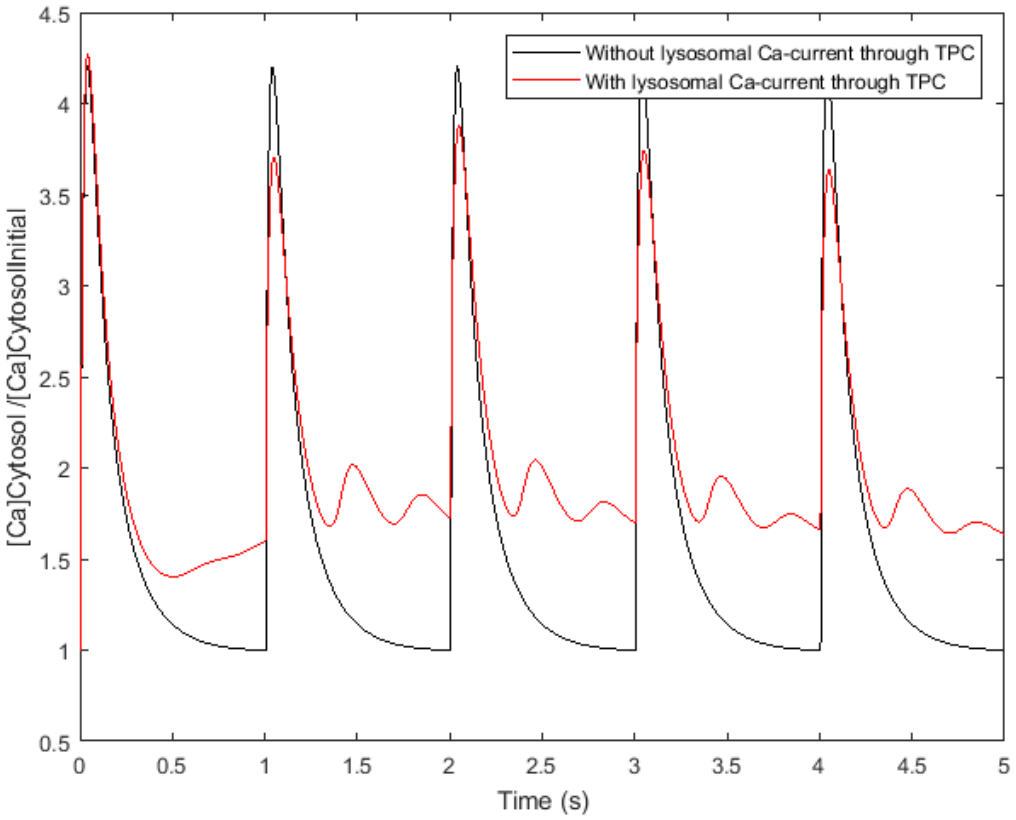


Figure 4.5: Results of comparing cytosol $Ca^{2+}$Wildtype myocardiocytes like in Morotti without lysosomal $Ca^{2+}$ current with cytosol $Ca^{2+}$ Wildtype myocardiocytes with lysosomal $Ca^{2+}$ current like in Model 1.

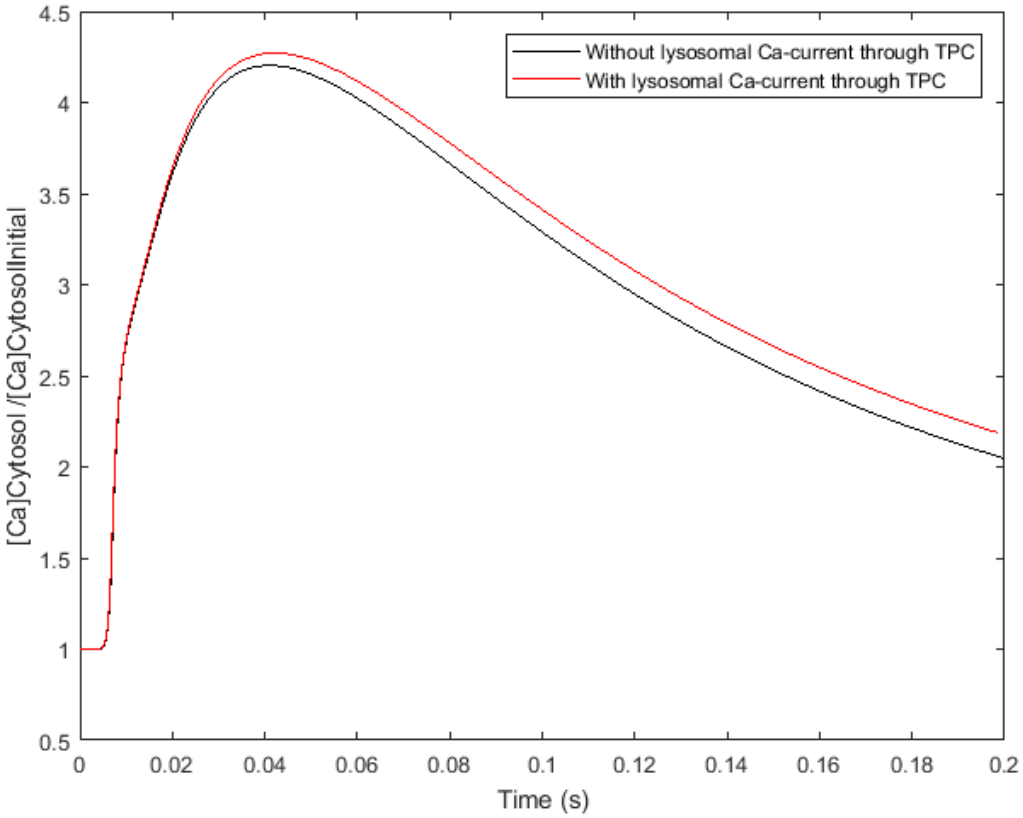


Figure 4.6: Results of comparing cytosol $Ca^{2+}$Wildtype myocardiocytes like in Morotti without lysosomal $Ca^{2+}$ current with cytosol $Ca^{2+}$ Wildtype myocardiocytes with lysosomal $Ca^{2+}$ current like in Model 1.

The Junction analysis holds, in some sort, as well for the Cytosol analysis. Main difference is the magnitude of the peaks and minimal output value. The maximal output value of the peak of the junction is around 470 while the maximal output value of the peak of the Cytosol is just 4.3. Also the steepness of the exponential decay is for the junction higher than for the cytosol. Both results come from the modeling of the junction to be much much smaller than the cytosol. Diffusion out of the junction will go much faster because of its relative small volume.
Now some comparison with the data-set without the lysosomal $Ca^{2+}$ current. After the peak in the first second, we see like the junction data-sets a divergence between the data-sets at around 0.2 seconds. The data grows again after 0.5 seconds unregulated. Each peak generated each second is lower than the data-set that excludes lysosomal $Ca^{2+}$ current. But what remarkably is, is that peaks (excluding the first peak) of the data-set that includes lysosomal $Ca^{2+}$ current are not constant but tend to fluctuate at an output value of 3.7. Once again we see the two normal-distribution-like tops that we have seen in the data-set from the junction that included lysosomal $Ca^{2+}$ current (see Figure (4.6)).

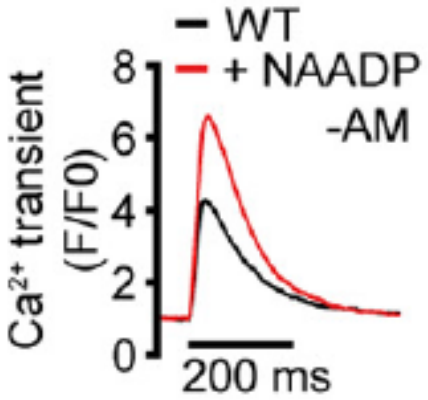


Figure 4.7: Shows $Ca^{2+}$ transient in Wildtype myocardiocytes and Wildtype myocardiocytes stimulated with 240 $nM$ NAADP-AM from [Capel et al., 2015].

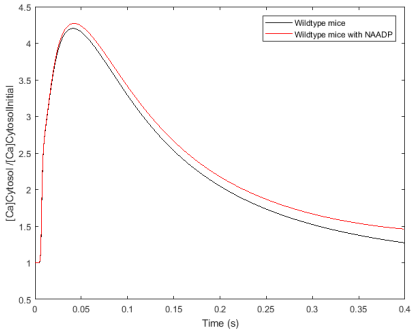


Figure 4.8: Results of scaled $Ca^{2+}$ concentration in the cytosol of Wildtype myocardiocytes and Wildtype myocardiocytes stimulated with 240 $nM$ NAADP.

In Figure (4.8) we can see our attempt on replicating the experimental data of Figure (4.7). If we compare the Wildtype myocardiocytes data from both figures, we can see they both grow exponentially to an out put peak and then exponentially decay. This is how we expected it and how it should be, as our Wildtype myocardiocytes data-set was from [Morotti et al., 2014], confirmed to correspond to Wildtype experimental data-sets. Next, we compare our data-set of Wildtype myocardiocytes after application of NAADP to the experimental data-set of [Capel et al., 2015] after application of NAADP-AM. Firstly we notice that our data-set has relatively smaller peak than the data-set of [Capel et al., 2015] after application of NAADP-AM, compared with the Wildtype myocardiocytes in both plots. Both the peaks of Wildtype myocardiocytes and Wildtype myocardiocytes with application of NAADP seem to reach their maximum at the the same time of about, 0.05 seconds. We compare this to the experimental data-set of [Capel et al., 2015] and conclude that both peaks reach their maximum at roughly 0.05 seconds. We conclude that our peak time-mark does correspond to the time-mark found in the experimental data-set of [Capel et al., 2015].
We can see some difference in the data-sets with NAADP(-AM). The difference between our data-sets seems to become slowly bigger after the peak at time-mark 0.05 seconds. This does not apply for the experimental data-sets of [Capel et al., 2015]. The difference starts out relatively big at the peak time-mark and then becomes smaller as time progresses.

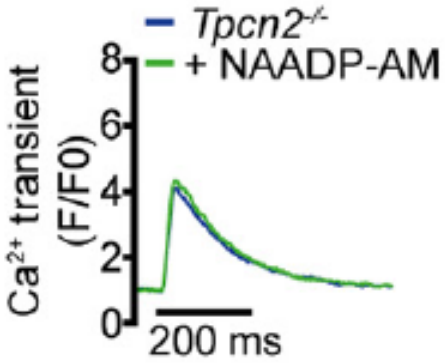


Figure 4.9: Shows $Ca^{2+}$ transient in TPC-knockout myocardiocytes and TPC-knockout myocardiocytes stimulated with 240 $nM$ NAADP-AM.

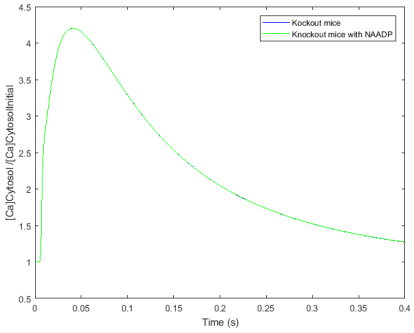


Figure 4.10: Results of scaled $Ca^{2+}$ concentration in the Cytosol of TPC-knockout myocardiocytes and TPC-knockout myocardiocytes stimulated with 240 $nM$ NAADP.

In Figure (4.9) we can see the influence of NAADP-AM on TPC-knockout myocardiocytes. We simulated these results from [Capel et al., 2015] (see Figure (4.10)). Our results correspond perfectly: NAADP does not have any influence on the Cytosol $Ca^{2+}$ concentration from TPC knockout myocardiocytes. From [Capel et al., 2015] we know that the TPC is essential for the lysosomal $Ca^{2+}$ current. This way, we mathematically validated this conclusion in [Capel et al., 2015].

## 4.2 Model 2

We also tested some scenarios for model 2 and compared them with results from model 1 and extended the timescale. Consequently, we can see if the changing of the parameter lysosomal $Ca^{2+}$ to variable has significant influence on the $Ca^{2+}$ concentrations. These plots can be seen in Figure (4.11), (4.12) and (4.13).

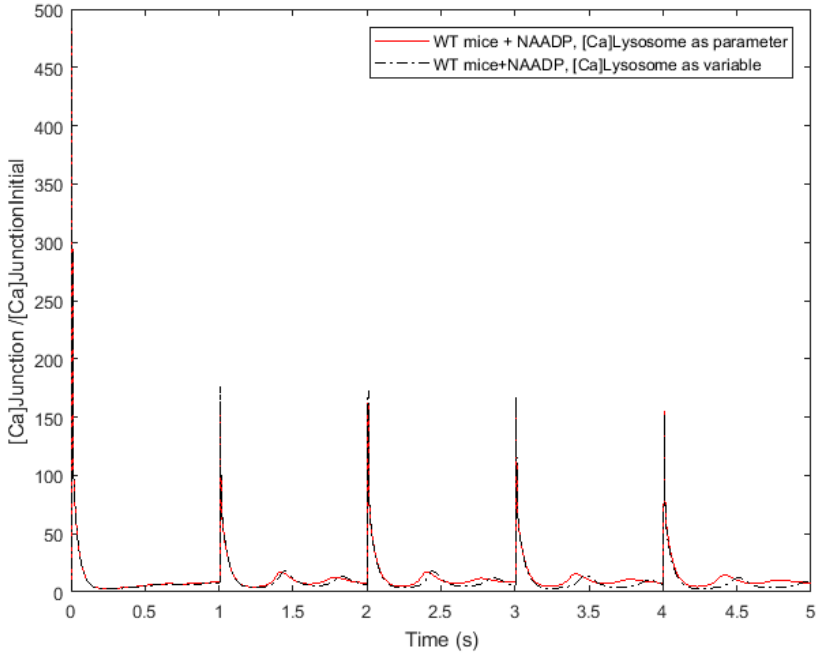


Figure 4.11: Difference between models 1 and 2, under stimulation of 240 $nM$ NAADP.

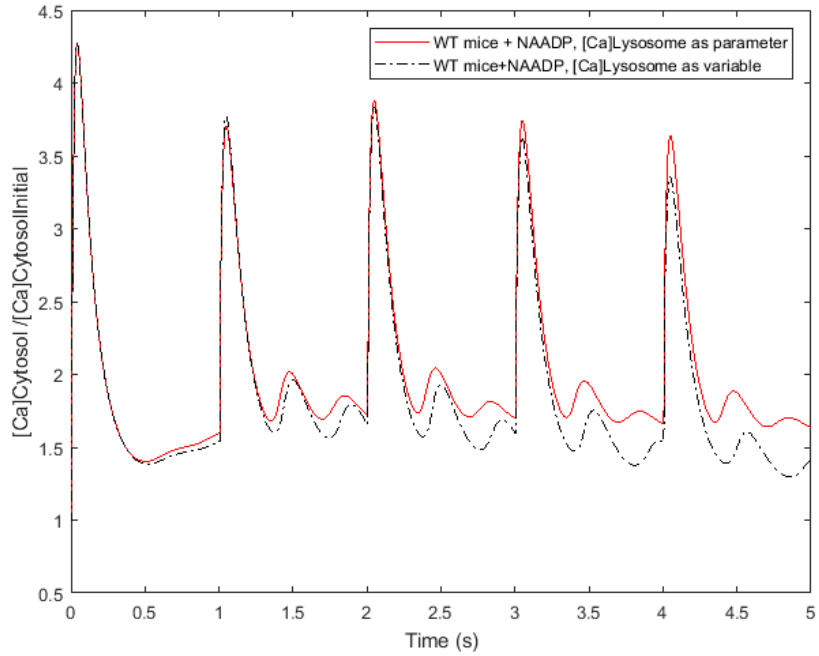


Figure 4.12: Difference between models 1 and 2, under stimulation of 240 $nM$ NAADP.

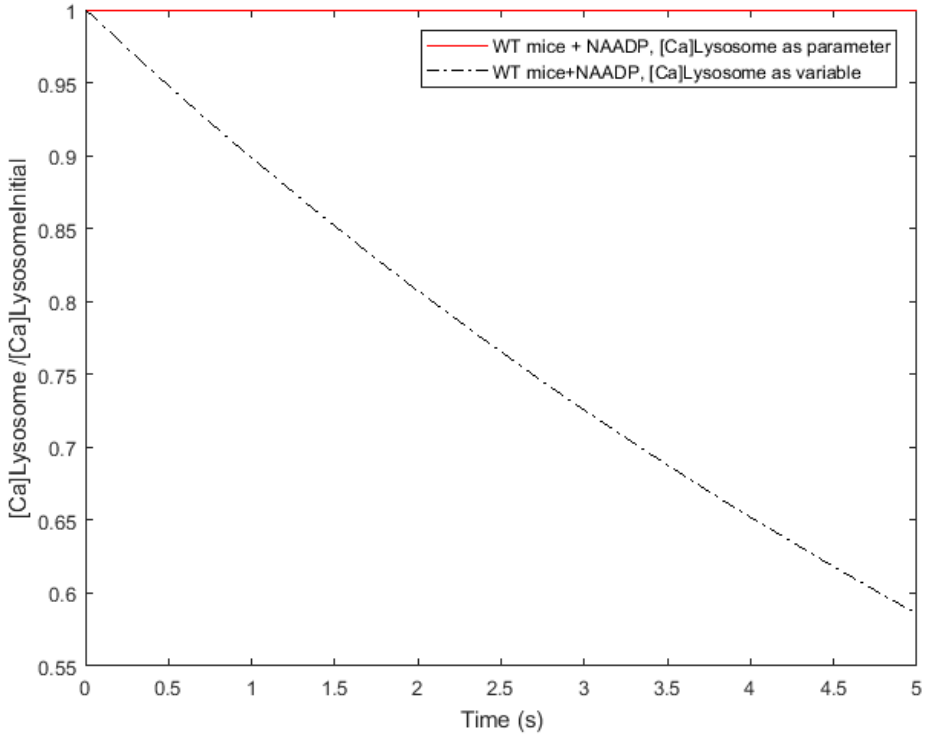


Figure 4.13: Difference between models 1 and 2, under stimulation of 240 $nM$ NAADP.

We can conclude from Figure (4.11) and (4.12) that seems to give overall higher output values. The peak of contraction are higher than those of model 1, which is makes model 1 better in this point. But model 1 is also in the intervals between these peaks of contraction consistently higher than model 2. This is not optimally, as both should in this interval go towards 1, as we have seen in Figure (4.3) and (4.5) from the data-set from [Morotti et al., 2014]. But from Figure (4.12), it seems that after each peak of the contraction of model 2 the normal-distribution-like peaks go down in value. This gave us the indication that they might flatten out. Therefore we tried simulating over a longer period of time (60 seconds), which results can be seen in Figure (4.14), (4.15) and (4.16).

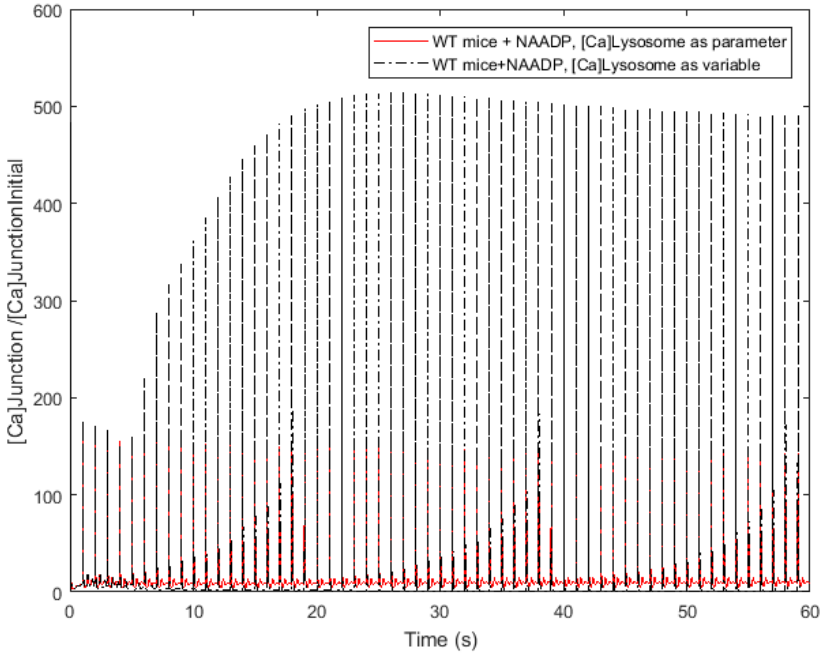


Figure 4.14: Difference between models 1 and 2, under stimulation of 240 $nM$ NAADP.

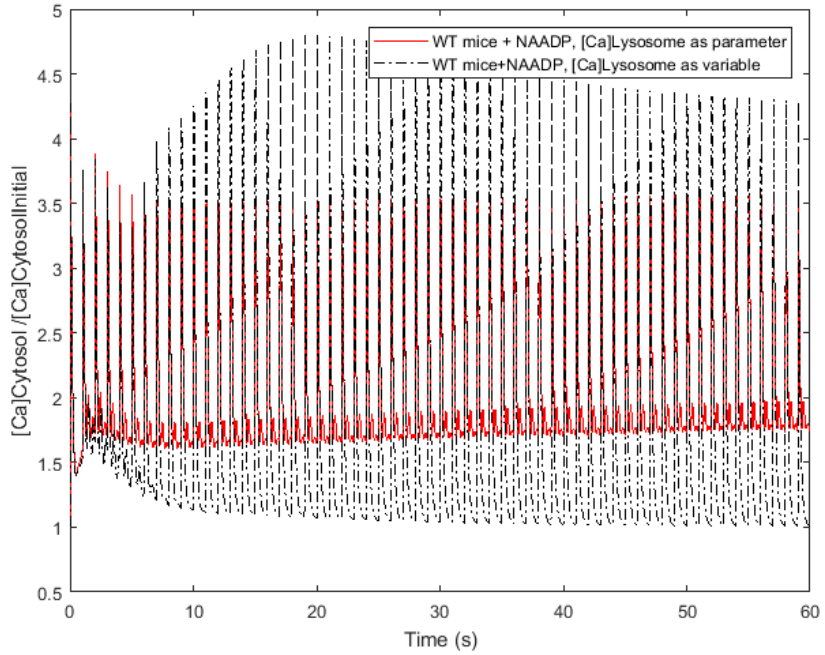


Figure 4.15: Difference between models 1 and 2, under stimulation of 240 $nM$ NAADP.

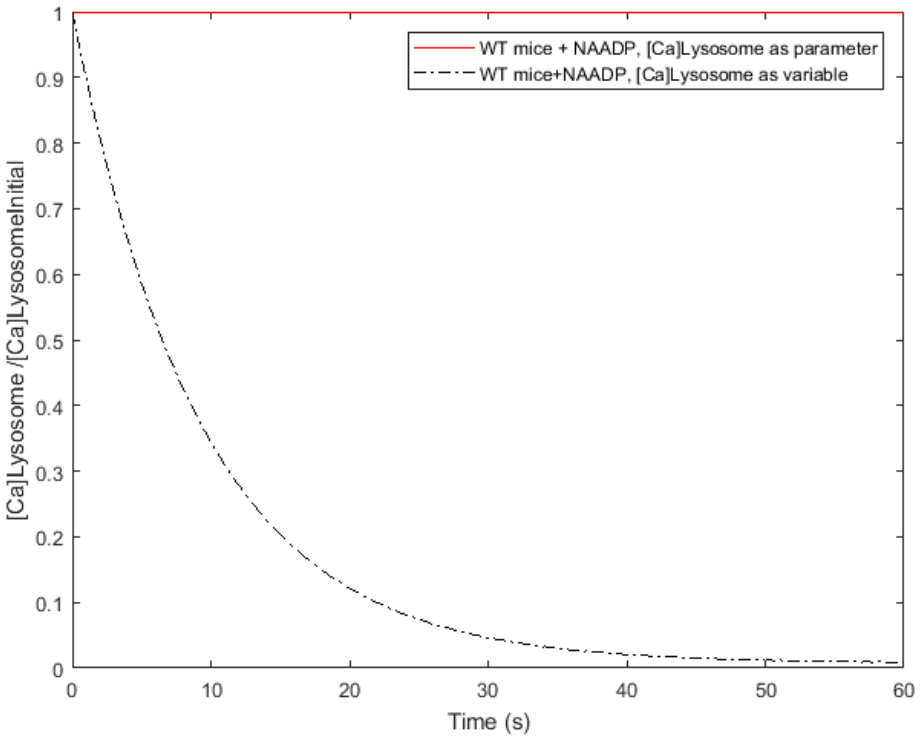


Figure 4.16: Difference between models 1 and 2, under stimulation of 240 $nM$ NAADP.

Not only do we see that these normal-distribution-like peaks indeed flatten out. But surprisingly, the behavior of the contraction peaks also change! Both the Junction and Cytosol contraction peaks grow towards a maximum peak, then decay a bit and then the peaks seem to become as high as our first peak of the plots. The Lysosome $Ca^{2+}$ concentration does still decay, and we can see clearly that this goes towards zero. Does the height of the peak of the model 2 stay constant? To find out we extended the timescale some more to 300 seconds.

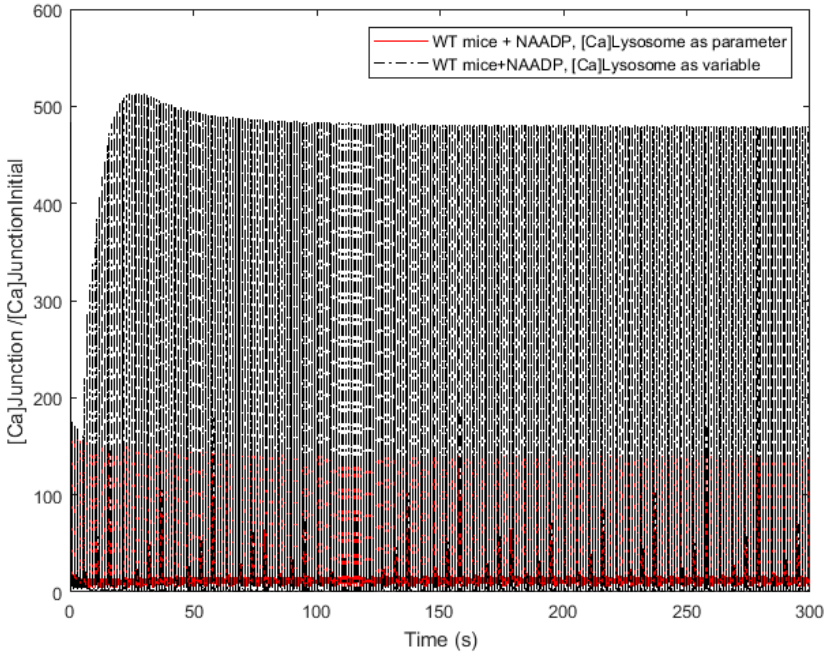


Figure 4.17: Difference between models 1 and 2, under stimulation of 240 $nM$ NAADP.

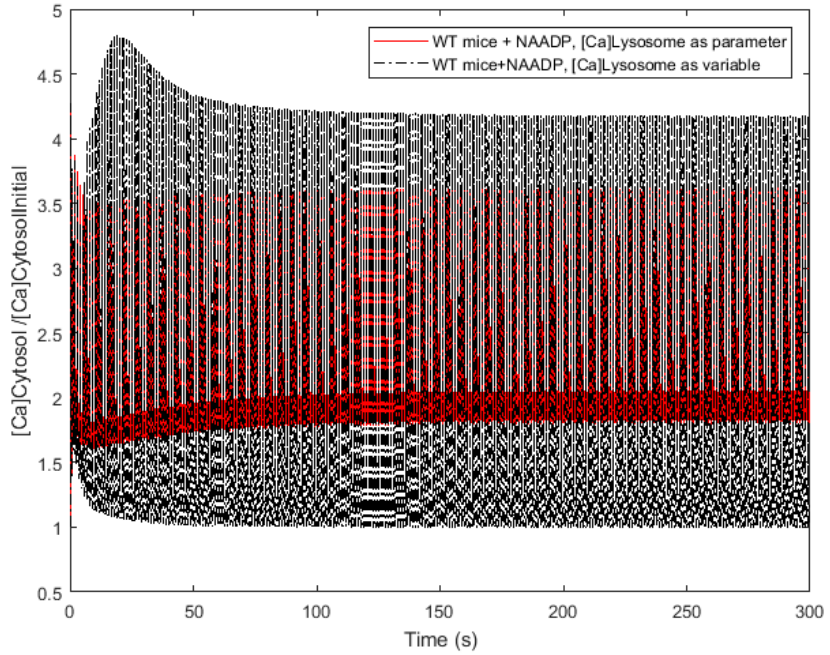


Figure 4.18: Difference between models 1 and 2, under stimulation of 240 $nM$ NAADP.

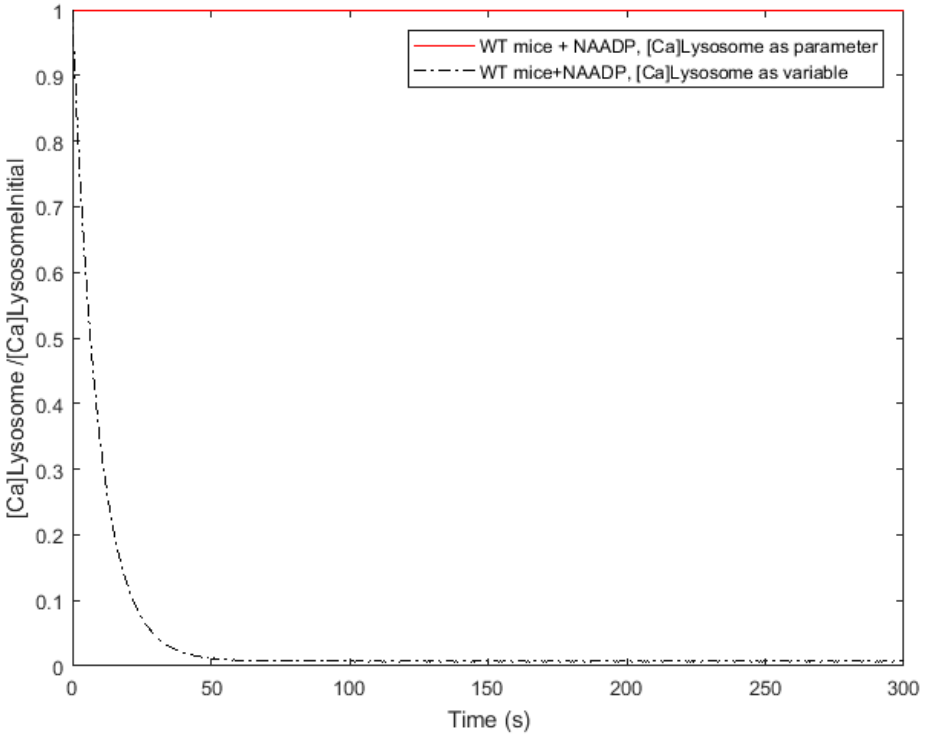


Figure 4.19: Difference between models 1 and 2, under stimulation of 240 $nM$ NAADP.

We can indeed conclude that the peaks of model 2 seem to converge to, and more specific, to the values 470 for the Junction and 4.3 for the Cytosol that we have seen in Figure (4.4) and (4.6). What is noteworthy is that the peaks of model 1 converge as well, but not to the values of 470 and 4.3. This can be seen clearly in the zoomed-in versions of Figure (4.17) and (4.18), see Figure (4.20) and (4.21).

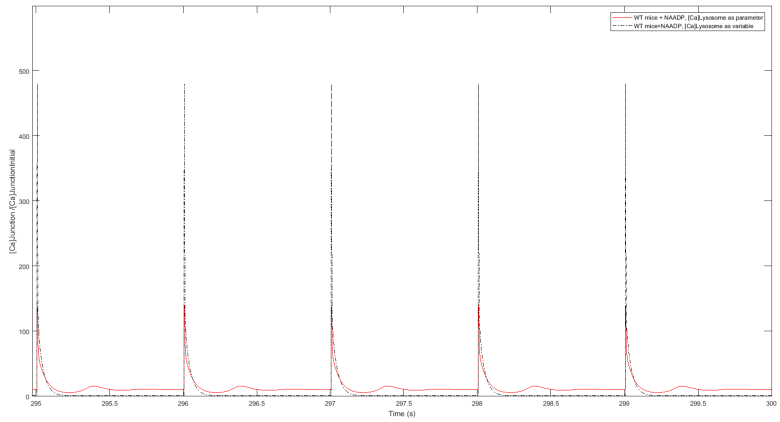


Figure 4.20: Long term difference between models 1 and 2, under stimulation of 240 $nM$ NAADP.

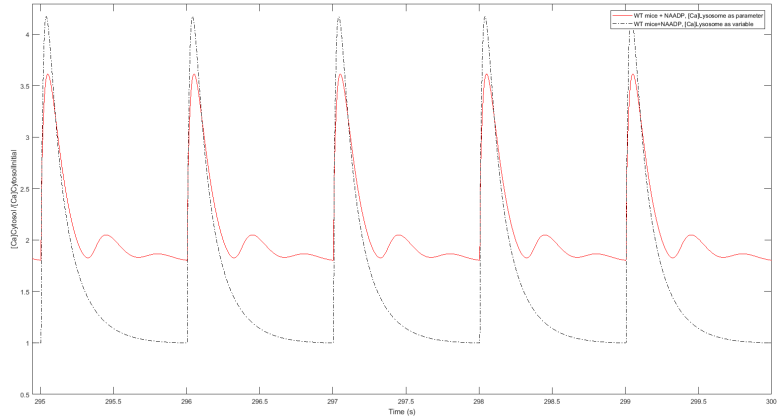


Figure 4.21: Long term difference between models 1 and 2, under stimulation of 240 $nM$ NAADP.

This convergence might be because we have an uniform stimulation of NAADP. After the short irregularity, caused by the stimulation, the cell can adjust to this stimulation and return back to its usual periodic contraction peaks and concentration levels. This shows the great adaptivity of the system under influences from in- and outside.

## 4.3 More optimization of the models

So how can we optimize our models. What we suggest first to optimize in the model, is to extend the Lysosome compartment with the re-uptake of $Ca^{2+}$ by the $H^{+}$-$Ca^{2+}$ exchanger in the lysosome-membrane which can be seen in Figure (1.6). The Lysosome $Ca^{2+}$ concentration depletes over time (see Figure (4.19)), which makes sense as this exchanger was not modeled. This depletion must have negative effect on the lysosomal $Ca^{2+}$ current, because this current is dependent of the Lysosome $Ca^{2+}$ concentration (see Equation (2.9)), although this negative effect can not be effectively be concluded from our results. When this exchanger could be modeled, maybe by the same methods explained in Section (2.3) we could describe the behavior of this Lysosome $Ca^{2+}$ concentration in a better way.
To optimize the results we need to add some more physical information to our model. In [Aston et al., 2017] was suggested with visual observations that the lysosome not only is located near the Junction that we used in models 1 and 2, but that it is also located on the other side of the SR (see Figure 4.22).

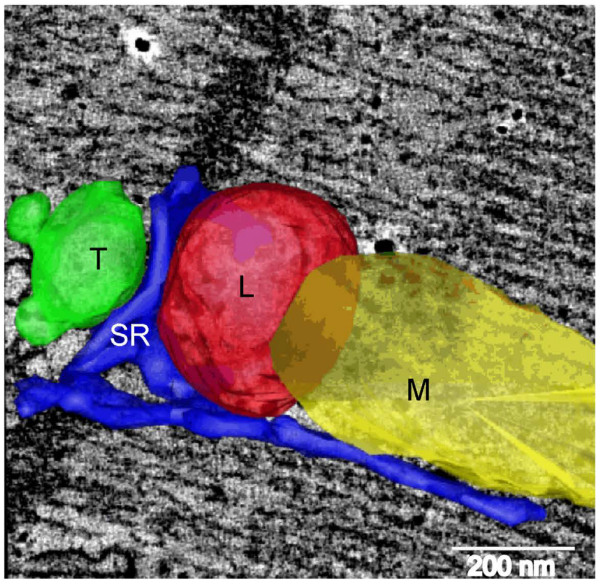


Figure 4.22: 3D Electron Tomography reconstruction of rabbit ventricular myocardiocytes, from [Aston et al., 2017].

Therefore we suggest to not only have a Junction like in models 1 and 2, but to create a new Junction (which we refer here to as Cleft) on the other side of the SR near the SERCA. This does make sense, as $Ca^{2+}$ has been observed to have effect on the RyR in the modeled Junction and on the SERCA. Previously, the SERCA was located into the Cytosol, but with the addition of the suggestions of [Aston et al., 2017], we might model the SERCAs in the newly defined Cleft.
Then, this newly made model consisting of the Junction and the Cleft would be looking roughly like this.

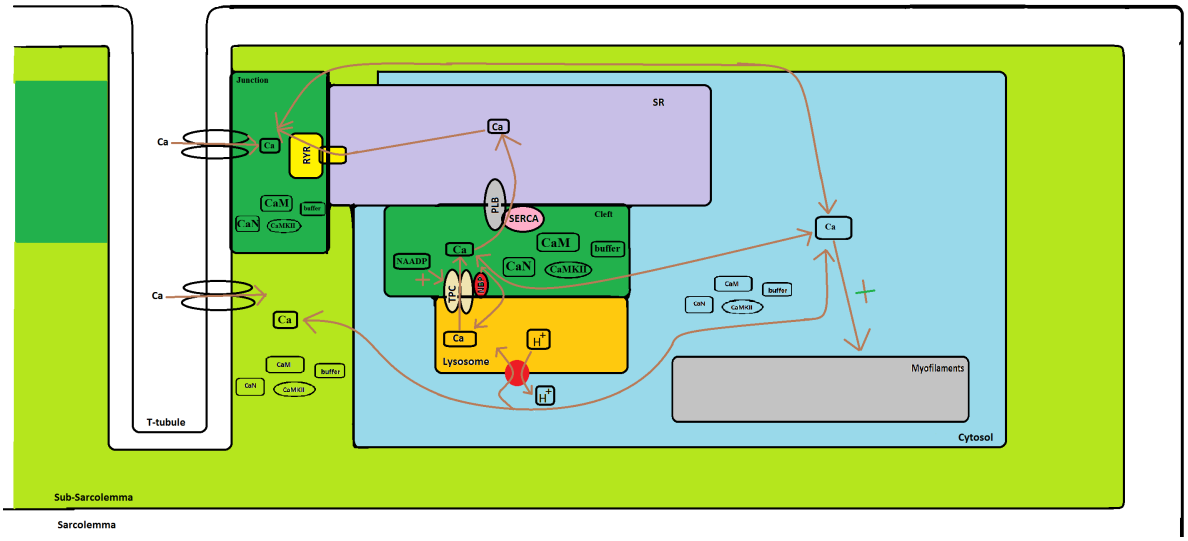


Figure 4.23: Suggestion on the newly made model for lysosomal $Ca^{2+}$ current including the Junction, the Cleft and the $H^{+}$-$Ca^{2+}$ exchanger.

In this model we suggest that the Lysosome forms a new Junction with the SR called the Cleft. This leads to a new compartment with new interactions with the other compartments. We suggest that the Cleft only interacts with the SR components like the SERCA, the Cytosol and the Lysosome. For the Cleft compartment compartment-specific interactions should be modeled, like buffers. This can be done by referring back to [Morotti et al., 2014]. We might keep the Lysosomal $Ca^{2+}$ concentration again fixed (or as a variable, depending on workload) in time while we let the Cleft $Ca^{2+}$ concentration be a new variable $Ca_{Cle}$. We might assume that the dimensions of the Cleft will be the same as those of the Junction. This means we will have to define some new parameters for the Cleft with similar values as those of the Junction. This leads to a new differential equation, namely for the Cleft $Ca^{2+}$ concentration, and a differential equation for the lysosomal $Ca^{2+}$ as well if we choose this to be a variable.

We have used some methods that do not meet the standard method of fitting to data. In specific taking the average of two earlier found parameters (see Table (3.1)) and loosely setting the variable $I_{Ca,tot,Lys} = 0$ for all time. Therefore when this new model will be used in the future, these two for sure should be reevaluated.

# Bibliography

[Allbritton et al., 1992] Allbritton, N. L., Meyer, T., and Stryer, L. (1992). Range of messenger action of calcium ion and inositol 1,4,5-trisphosphate.

[Aston et al., 2017] Aston, D., Capel, R. A., Ford, K. L., Christian, H. C., Mirams, G. R., Rog-Zielinska, E. A., Kohl, P., Galione, A., Burton, R. A. B., and Terrar, D. A. (2017). High resolution structural evidence suggests the sarcoplasmic reticulum forms microdomains with acidic stores (lysosomes) in the heart.

[Briggs and Haldane, 1992] Briggs, G. E. and Haldane, J. B. S. (1992). A note on the kinetics of enzyme action. *Biochemical Journal*, 19(2):338–339.

[Capel et al., 2015] Capel, R. A., Bolton, E. L., Lin, W. K., Aston, D., Wang, Y., Liu, W., Wang, X., Burton, R.-A. B., Bloor-Young, D., Shade, K.-T., Ruas, M., Parrington, J., Churchill, G. C., Lei, M., Galione, A., and Terrar, D. A. (2015). Two-pore channels (tpc2s) and nicotinic acid adenine dinucleotide phosphate (naadp) at lysosomal-sarcoplasmic reticular junctions contribute to acute and chronic $\beta$-adrenoceptor signaling in the heart.

[de Jong, 2016] de Jong, S. (2016). A mathematical model for calcium dynamics in atrial myocytes.

[Fameli et al., 2014] Fameli, N., Ogunbayo, O. A., van Breemen, C., and Evans, A. M. (2014). Cytoplasmic nanojunctions between lysosomes and sarcoplasmic reticulum are required for specific calcium signaling.

[Hodgkin and Huxley, 1952] Hodgkin, A. L. and Huxley, F. (1952). A quantitative description of membrane current and its application to conduction and excitation in nerve. *J. Physiology*, 117:500–544.

[Morotti et al., 2014] Morotti, S., Edwards, A. G., McCulloch, A. D., Bers, D. M., and Grandi, E. (2014). A novel computational model of mouse myocyte electrophysiology to assess the synergy between $na^+$ loading and camkii.

[Penny et al., 2014] Penny, C. J., Kilpatrick, B. S., Han, J. M., Sneyd, J., and Patel, S. (2014). A computational model of lysosomeer $ca^2+$ microdomains.

[Pitt et al., 2010] Pitt, S. J., Funnell, T. M., Sitsapesan, M., Venturi, E., Rietdorf, K., Ruas, M., Ganesan, A., Gosain, R., Churchill, G. C., Zhu, M. X., Parrington, J., Galione, A., and Sitsapesan, R. (2010). Tpc2 is a novel naadp-sensitive $ca^{2+}$ release channel, operating as a dual sensor of luminal ph and $ca^{2+}$.

[Shannon et al., 2004] Shannon, T. R., Wang, F., Puglisi, J., Weber, C., and Bers, D. M. (2004). A mathematical treatment of integrated ca dynamics within the ventricular myocyte.